Winding and Curing Stress Analysis of Filament Wound Composites by Finite Elements

by

John Christopher Johnson

Thesis submitted to the Faculty of the

Virginia Polytechnic Institute and State University

in partial fulfillment of the requirements for the degree of

Master of Science

in

Mechanical Engineering

APPROVED:

Dr. Charles E. Knight, Chairman

Dr. Alfred C. Loos

Dr. Hamilton H. Mabie

January, 1986

Blacksburg, Virginia

Winding and Curing Stress Analysis of Filament Wound Composites by Finite Elements

by

John Christopher Johnson

Dr. C. E. Knight, Chairman

Mechanical Engineering

(ABSTRACT)

Filament wound composite structures are becoming more and more attractive to designers in the aircraft and aerospace industries due to increasing strength- and stiffness-to-weight ratios and falling fabrication costs. However, the interaction of some of the manufacturing process variables such as mandrel stiffness and thickness, winding tension and pattern, and cure cycle characteristics can lead to common defects such as delamination, matrix cracking and fiber buckling.

A model of the filament winding process was developed to better understand the behavior of wound structures during fabrication. Specifically, the residual stress state at the end of winding, heat-up and cool-down was determined. This information is important because adverse stress states are the mechanism through which the process variables cause fabrication defects.

The process model utilized an incremental finite-element analysis to simulate the addition of material during winding. Also, the model was refined and extended to include changes that occur in the material behavior during the cure.

A fabrication analysis was performed for an 18 in. (457 mm) graphite/epoxy filament wound bottle. Two different mandrel models were examined, a rigid steel and a soft sand/rubber mandrel. At the end of winding, the composite layers in the model retained all of their initial winding tension for the steel mandrel but did exhibit significant loss of tension for the sand/rubber mandrel. The composite layers experienced a large increase in tension during heating for the steel mandrel but showed no significant recovery of tension for the sand/rubber system.

ACKNOWLEDGEMENTS

I would first like to thank Dr. Charles E. Knight for his serving as my graduate committee chairman. His guidance and encouragement has made the completion of this thesis possible.

Special thank are in order to Dr. Alfred C. Loos and Dr. Hamilton H. Mabie for serving on my graduate committee, and for taking the time to answer my questions.

In addition, I want to express my gratitude to the following for their support during the past 16 months.

Barry Gardiner, Tony Spagnuolo, Kenny Elliot and Ron Rorrer, who were always willing to share in my sense of adventure. Their friendship will be sorely missed.

Jim Meeks, Eric Jennings, Suzy Carr, and David Cook, whose optimism and friendship always kept me in good spirits.

My parents, Mr. and Mrs. John G. Johnson, whose love and understanding provided the foundation for my education.

Morton Thiokol Inc. for funding the research project on which I worked.

The Martin Marietta Corp. for their patience and for giving me the opportunity to enjoy the benefits of hard work, where its warm.

And finally, I want to thank Jeanne Furlong for her companionship and unending faith. I will forever be indebted to you.

TABLE OF CONTENTS

LIST OF ILLUSTRATIONS

LIST OF TABLES

NOMENCLATURE

{b}	Vector of body forces
[B]	Matix of strain shape functions
[C]	Material compliance matrix
d_i	i^{th} displacement degree of freedom
[D]	Material stiffness matrix
E	Young's modulus of elasticity
F_i	i^{th} nodal force or moment
{F}	Vector of element nodal forces
G	Modulus of rigidity
H	Weighting coefficients
I	Potential energy of element
[J]	Jacobian matrix
K_{ij}	stiffness coefficients
[K]	element stiffness matrix
N	Shape function
[N]	Matrix of shape functions
P.E.	Potential energy of external loads
r	Radial coordinate
r_i	Radial nodal point coordinate
r,z,t	Global axisymmetric coordinate system.
{T}	Vector of surface tractions
$[T_i]$	i^{th} stress transformation matrix

$[T_m]$	Master stress transformation matrix
u	Radial displacement
u_i	i^{th} nodal point displacement in r direction
$\{u\}$	Vector of interpolated displacements u and v in element
v	Axial displacement
v_i	i^{th} nodal point displacement in v direction
vol	Element volume
z	Axial coordinate
z_i	Axial nodal point coordinate
$\{\alpha\}$	Vector of thermal expansion coefficients
ε	strain
$\{\varepsilon\}$	Strain tensor
ξ,η	Natural coordinates
ν	Poisson's ratio
σ	stress
$\{\sigma\}$	Stress vector
1,2,3	Fiber coordinate system

Superscript

e	Element
t	Transpose
th	Thermal
*	Inverse
'	Transformed
+/-	Plus or minus fiber band

Subscripts

r	Radial direction
t	Tangential direction
z	Axial direction
o	Initial condition
m	Mechanical component of stress

1 INTRODUCTION

The advantages of using fiber reinforced composite structures have long been recognized by the aerospace industry. Superior strength- and stiffness-to-weight ratios, excellent fatigue characteristics and thermal stability are several of these advantages. Commercial and military aircraft are making extensive use of fiber reinforced composites in structural components to reduce aircraft weight. The weight savings increase payload and range limits making the aircraft more fuel and cost efficient. All-composite airframes are currently being developed and will enter the market shortly. Modern spacecraft have utilized composites in a similar manner. High strength and low weight primary structures and motor cases have increased payload capacity. For satellites using solid fuel upper-stage boosters, a significant reduction of launch weight through the use of composite motor cases will result in enormous deployment cost savings. The fabrication of these composite structures is a complex process that is divided into two broad categories: (1) lay-up structures such as aircraft wing and control surfaces and (2) filament wound structures such as rocket motor cases.

In the case of filament wound structures the quality and performance of the final structure depends upon the interaction of several process and design variables. For example, the mandrel thickness and composition, the composite wall thickness, the winding tension, and the cure cycle characteristics all greatly affect the strength and reliability of the final structure in service. In particular, all these variables influence the level of residual stress in the composite structure. The state of residual stress is important because many of the defects that occur during fabrication, e.g. delamination and matrix cracking, are caused by adverse residual stresses. Therefore, a good understanding of the effect these variables have on the level of residual stress found in a filament wound structures is important if accurate strength predictions are to be made.

Although an enormous amount of literature has been published dealing with finite-element analysis (one computer search turned up over 14,000 citations), there is not an abundance of literature that deals directly with fabrication stresses in filament wound composites.

Knight and Leavesley [1] present a detailed review of some of the literature that deals with finite-element analysis of wound structures. Their work lead to the development of the finite-element program COMSPH. This program was used to study the interaction of mandrel stiffness and winding tension on the residual state of stress in a spherical pressure vessel. The winding process was modeled by performing an incremental analysis that simulated the addition of material to the model. A similar approach was used by Clough and Woodward [2] and by Duncan and Clough [3] who reported that an incremental analysis of the construction of earth embankments generated results that were closer to measured values of stress and displacement than for a one step load analysis.

Further background for Knight and Leavesley's work was a study performed by Dobie, Knight and Leavesley [4] which examined the effect that residual strain in the composite layers of a thin ring had on the predicted performance of the ring under load. Dobie, Knight and Leavesley found that there was a hyperbolic relationship between the spool tension measured on the winding apparatus and the residual tension in the fiber layer just after being wound onto the mandrel. Using this relationship and a specialized finite-element program (COMCYL) the residual stress-strain state in the composite ring was determined.

Knight and Leavesly's [1] work predicted that the winding process would cause some of the inner fiber elements to exhibit compressive fiber direction strains in a spherical pressure vessel wound in the delta-axisymmetric pattern. However, after integrating over a complete circular winding circuit, they found that none of the layers experienced total loss of winding tension.

The principles of classical lamination theory were used in their analysis. In other words, no attempt was made to account for the fact that the fiber bands making up the composite structure are free to displace relative to each other in the wet winding process. Also, no attempt was made to predict the behavior of the model during cure.

The residual stress in composite rings and cylinders was examined by Tarnopol'skii, et. al., [5] and by Uemura, et. al., [6]. Tarnopol'skii developed an analytical model based on equilibrium equations and compatibility of strains while Uemura used a microscopic analysis to study the interaction of the fiber and matrix during cure. Neither utilized the finite-element method, but both reported that the stresses generated in the composite fibers during cure are significant and should be taken into account when studying the fabrication process.

This study undertakes the development of an analytic model of the manufacturing processes involved in the fabrication of filament wound structures. Recent work by Knight and Leavesley [1] is used as the foundation for this model.

A computer program developed by Knight and Leavesley will be refined to reflect the change in material behavior before and after cure by providing both uncured and cured stress computation algorithms and material models. Also, the program will be extended to include the thermal stresses generated during the cure.

The new model is then used to examine the effects of design and process variables on the residual stress state in a filament wound vessel.

2 FILAMENT WINDING PROCESS AND SIMULATION

2.1 FILAMENT WINDING PROCESS

The filament winding process involves winding a high strength fiber yarn impregnated with an epoxy resin onto a rotating mandrel form illustrated in Fig. 1. Layer after layer is applied to the mandrel to build up the axisymmetric structure to the designed wall thickness. Each layer is wound onto the mandrel at a predetermined wrap angle and tension level. The wrap angle varies from 0° for hoop wound layers to 90° for polar layers while the tension assures that the fibers are wound onto the mandrel straight. When all the layers have been applied to the mandrel, the structure is then cured. During cure, the structure is heated and the resin matrix undergoes polymerization. The structure is then cooled and the mandrel removed if it is not an integral part of the structure.

The above is a very simple description of the filament winding process. The actual process is a combination of many intermediate processes. Although including all the intermediate processes is beyond the scope of this work, several intermediate processes do make significant contributions to the residual state of stress. These processes are: (1) relaxation of fiber tension due to mandrel deflection, (2) relaxation of fiber tension due to resin flow, (3) changes in material properties and behavior when the resin undergoes polymerization, and (4) constrained thermal expansion (contraction) upon cooling. These four intermediate

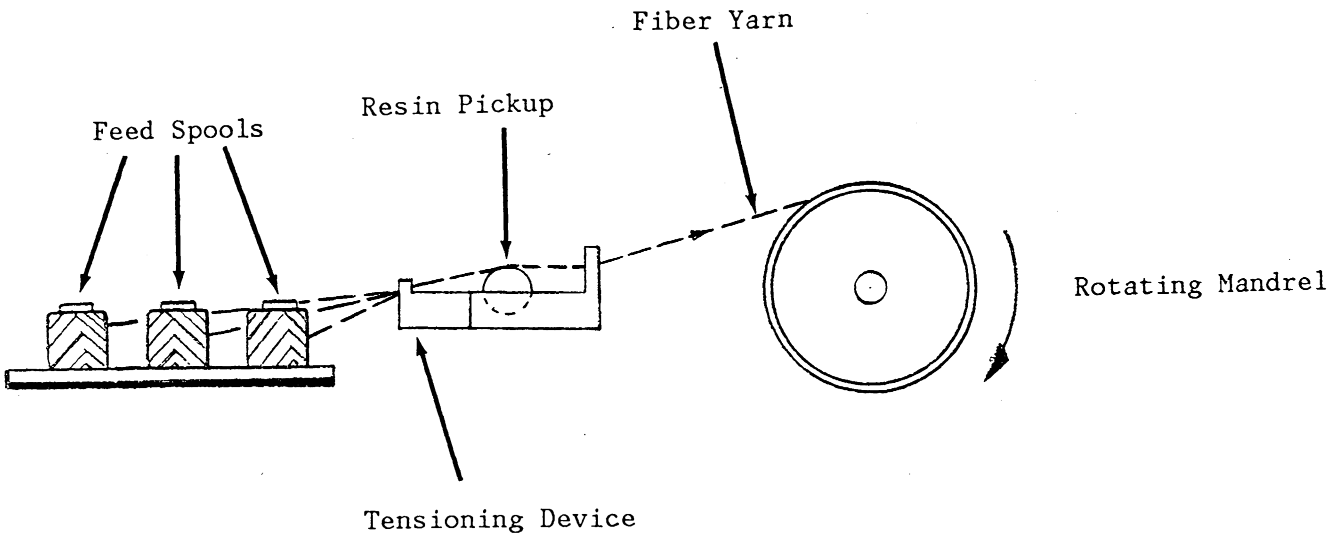

Figure 1. Schematic of the filament winding process.

processes describe mechanisms for loss of winding tension and are elaborated upon in the following paragraphs.

After the first layer is applied, the mandrel experiences an external pressure due to the winding tension. The mandrel deflects inward under the influence of this pressure. This deflection reduces the tensile strain in the fiber layer. The reduction in tensile strain is accompanied by a loss of tension in that layer. When the second layer is applied, the mandrel again deflects inward, further reducing the first layer's strain as well as some in the second layer. This sequence of events is repeated for each additional layer.

Also contributing to tension loss in the fiber layer is resin flow. In the wet winding process the resin matrix is a viscous fluid that is carried to the structure on the fiber yarn. After several layers have been applied to the mandrel, the external pressure due to winding tension causes the resin in the underlying layers to squeeze out of the composite. The bulk motion of the resin allows the fiber layers to migrate inward reducing the fiber strain. Again, the sequence of events is repeated for additional layers. The effects of both mandrel deflection and resin flow become more evident as wall thickness increases.

When the structure enters the curing stage of fabrication, the radial stiffness properties of the composite layers change under the influence of the resin viscosity. During the heating cycle, the resin viscosity decreases. This initial decrease in viscosity reduces the radial stiffness and accelerates resin flow. Polymerization is accompanied by an increase of both resin viscosity and radial stiffness as the resin reaches the gel point. The cooling cycle sees additional increases in viscosity and stiffness.

The generation of thermal stresses due to constrained thermal expansion (contraction) during cure can either contribute to or detract from the residual winding tension. The main factors that determine which effect the curing cycle will have are the coefficients of thermal expansion of the mandrel, composite layers and any other components present in the model.

The interaction of these four mechanisms can eventually cause the inner fiber layers to lose all their initial tension and try to support compressive loads in the fiber direction. If the resin matrix has not yet solidified, the fibers may buckle or become wavy. Layers consisting of buckled or wavy fibers will exhibit significant loss of the high-modulus fiber properties. The strength of these layers with total tension loss and buckled fibers will be degraded. Accurate prediction of the strength of a filament wound structure depends (among other factors) upon having a knowledge of any layers that exhibit degraded strength.

2.2 FINITE-ELEMENT SIMULATION

Several assumptions can be made that simplify the simulation of the filament winding process. For example, the modeling effort can be simplified by assuming that the structure is axisymmetric about the centerline and symmetric about the equatorial plane. Also, the fabrication process can be divided into stages so that simplifications can be made for one stage that would be inappropriate in another. The natural division of the filament winding process is into winding and curing stages.

Simulating the fabrication of a filament wound structure requires an incremental analysis. This requirement is primarily due to the built-up nature of the wound structure and the need to follow the changes in material properties and elastic behavior during cure. A finite-element program is well suited to modeling and analyzing this type of system.

A finite-element program currently exists which will perform an incremental analysis of the winding process for a filament wound sphere wound in a delta-axisymmetric pattern. This program (referred to as COMSPH) was used to study the interaction of winding tension and mandrel stiffness in relation to the loss of tension in the wound layers. The program simulates the addition of material by creating a finite-element model of the entire structure and then scaling down the stiffness matrices of those elements which have not yet been added to the model. As the analysis steps through the winding process, elements being added to the model have their stiffnesses restored to their full values. The program does not have the capability to follow the fabrication process through cure. Therefore, to simulate the entire fabrication process, a new program will be developed named WACSAFE (Winding and Curing Stress Analysis by Finite Elements) that incorporates most of the capabilities of COMSPH and also takes into account the generation of thermal stresses and strains during heating and cooling. In addition, some of the changes in material behavior that occur during cure will be considered. Also, some aspects of COMSPH will be generalized to include shapes other than the spherical shape generated by the delta-axisymmetric winding pattern.

After the necessary code modifications and additions have been completed, an interfacing program needs to be developed to enable finite-element models of filament wound structures developed at Morton Thiokol Inc. (Wasatch Division) to be run with the new finite-element code. The model provided by Morton Thiokol which is used as a test case in this work is an 18 in. (457 mm) graphite/epoxy filament wound bottle. Details of this model are presented in the model preparation chapter.

3 FINITE ELEMENT FORMULATION

3.1 INTRODUCTION

A general formulation of the finite-element method can be found in any introductory text on finite-element theory. Rather than present the entire formulation, only a brief discussion of those topics that relate directly to this research are presented. For a more complete formulation, the reader is referred instead to references [1 and 7-11]. Much of the following work is taken from Knight and Leavesley [1].

3.2 DISPLACEMENT METHOD

Several approaches are available for the elasticity formulation of the finite-element method. A separate formulation is required because of the vector nature of the field variables under consideration--stresses, strains, displacements. The commonly used approaches are: (1) the displacement method, (2) the force or stress method and (3) a mixed method. The displacement method is used because it is the easiest to apply and is the most widely accepted. Its application to elasticity problems is especially well suited because the principle of minimum potential energy can easily be applied using this approach.

The displacement method is based on an assumed displacement inside and along the element boundaries. The functions used to represent the displacements are chosen such that continuity inside and across interelement boundaries is maintained. These functions are referred to as interpolation functions. An element formulated with this continuity constraint is called a compatible element. Compatible elements will satisfy force equilibrium only at the element nodes; some local violations of force equilibrium are to be expected. However, force equilibrium will be satisfied in an overall sense.

Monitoring the displacement of the nodes results in one equation for each degree of freedom associated with that node. For an axisymmetric two dimensional problem, each node possesses two degrees of freedom, one being the displacement in the radial direction and the other being displacement in the axial direction. The displacement degrees of freedom and nodal forces are related through the following stiffness coefficients.

$$\begin{array}{ccccccccc} K_{11}d_1 & + & K_{12}d_2 & + & \cdots & + & K_{1n}d_n & = & F_1 \\ \vdots & & \vdots & & \cdots & & \vdots & & \vdots \\ K_{n1}d_1 & + & K_{n2}d_2 & + & \cdots & + & K_{nn}d_n & = & F_n \end{array} \qquad (1)$$

Equation 1 is written in matrix form as

$$[K]\,\{d\} = \{F\} \qquad (2)$$

where [K] - global stiffness coefficient matrix

{d} - vector of nodal displacements

[F] - vector of nodal forces

In the finite-element method, the stiffness coefficient matrix $[K^e]$ for each element is determined and then assembled into the global stiffness matrix.

3.3 ELEMENT FORMULATION

The element used in the finite-element program WACSAFE is the axisymmetric, quadrilateral, isoparametric element. This element was chosen because the development and accuracy of the element is well documented [5,6].

An element is referred to as isoparametric when the interpolating function used to describe displacements is also used to map the element shape in the global coordinate system (r,z), into a square element in a natural coordinate system (ξ,η). Hence the interpolating functions are called shape functions. The mapping is illustrated in Fig. 2. The shape functions in natural coordinates are

$$N_1 = \frac{1}{4}(1 - \xi)(1 - \eta) \qquad N_3 = \frac{1}{4}(1 + \xi)(1 + \eta) \tag{3}$$

$$N_2 = \frac{1}{4}(1 + \xi)(1 - \eta) \qquad N_4 = \frac{1}{4}(1 - \xi)(1 + \eta)$$

These polynomials are bilinear and therefore restrict the variation of displacement to a linear form along interelement boundaries. This assures that compatibility is maintained since the element boundaries will remain straight at all times as in Fig. 2. An element with linear shape functions is referred to as a linear element.

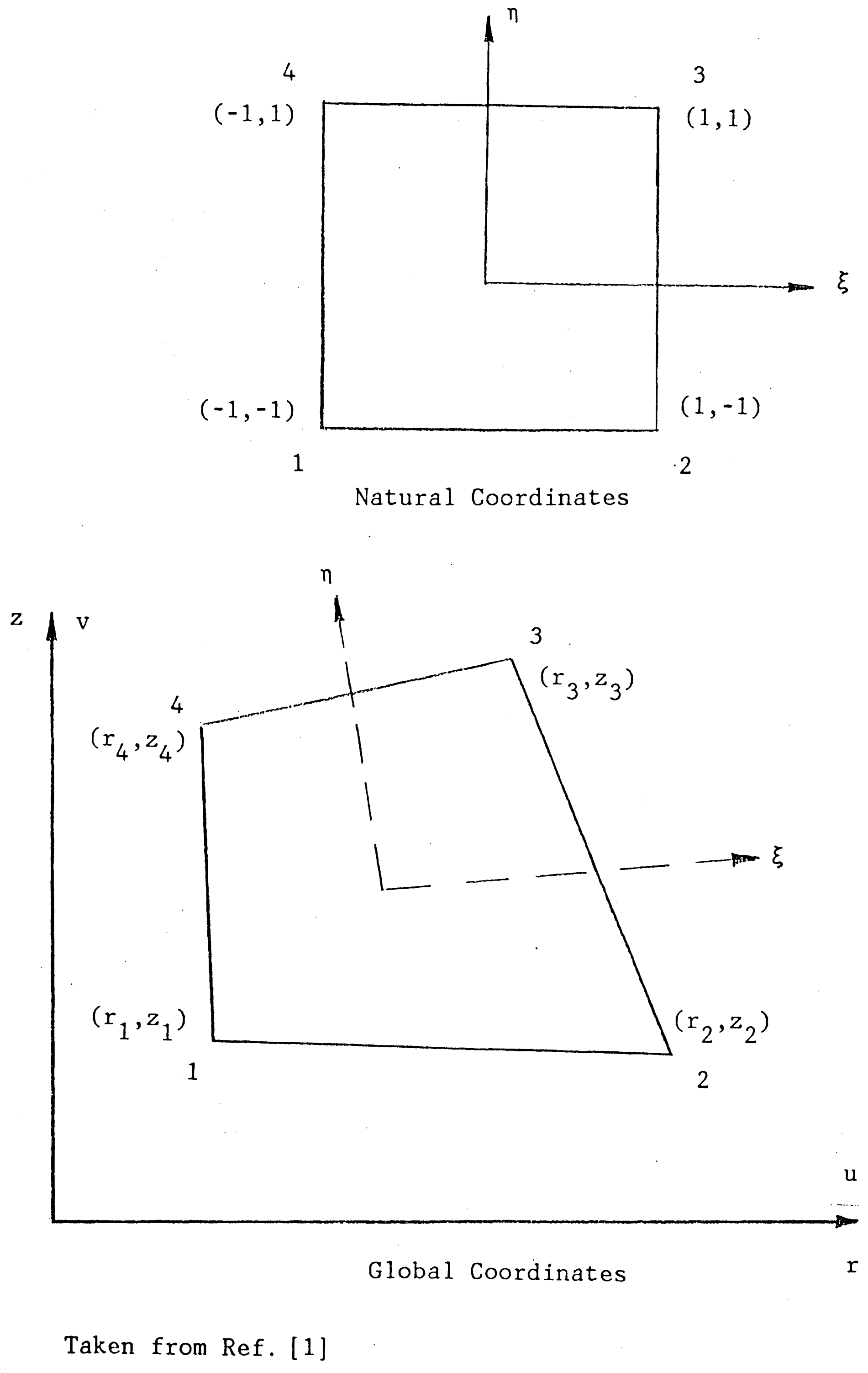

Figure 2. Mapping of element shape into natural coordinates.

The shape functions define the relationship between displacements in the two coordinate systems by the following summation.

$$u(\xi,\eta) = \sum_{i=1}^{4} N_i u_i \tag{4}$$

$$v(\xi,\eta) = \sum_{i=1}^{4} N_i v_i$$

where $u(\xi,\eta)$, $v(\xi,\eta)$ - interpolated displacement field

N_i - i^{th} shape function

u_i - displacement of node i in r direction

v_i - displacement of node i in z direction

Equation 4 also applies to the coordinate mapping because the element is isoparametric. Written in matrix notation the displacement relationship is

$$\{u\} = [N]\,\{d\} \tag{5}$$

where $\{u\}$ - vector of interpolated displacements u and v

$[N]$ - matrix of shape functions

$\{d\}$ - vector of nodal displacements, u_i and v_i

Earlier, the principle of minimum potential energy was referred to as a factor in choosing to use the displacement method. The reasoning behind that reference is that the solution to the differential equation governing a system is found when the potential or strain energy is minimized. Minimizing the potential energy involves taking the first variation and equating it with zero.

The potential energy in matrix form for an element, neglecting initial stresses, strains, tractions, and body forces, is

$$I^e = \frac{1}{2} \int_{vol} \{\sigma\}^t \{\varepsilon\} \, dvol \tag{6}$$

where I^e - potential energy for element (e).

$\{\sigma\}^t$ - transposed element stress tensor

$\{\varepsilon\}$ - element strain tensor

The strain tensor in Eq. 6 is written in terms of the stress tensor by using the orthotropic stress-strain relations.

$$\{\sigma\} = [D] \{\varepsilon\} \tag{7}$$

where $[D]$ - material stiffness matrix

The material stiffness matrix can be derived directly from the material properties or by deriving the material compliance matrix [S] and inverting to obtain [D].

For the orthotropic axisymmetric case, the symmetric material stiffness matrix is

$$[D] = \frac{1}{Div}\begin{bmatrix} E_r(1-\nu_{zt}\nu_{tz}) & E_z(\nu_{rz}+\nu_{rt}\nu_{tz}) & E_t(\nu_{rt}+\nu_{rz}\nu_{zt}) & 0 \\ & E_z(1-\nu_{rt}+\nu_{tr}) & E_t(\nu_{zt}+\nu_{zr}\nu_{rt}) & 0 \\ & & E_t(1-\nu_{rz}+\nu_{zr}) & 0 \\ & & & G_{rz} \end{bmatrix} \qquad (8)$$

where

$$Div = (1 - \nu_{rz}\nu_{zr} - \nu_{zt}\nu_{tz} - \nu_{tr}\nu_{rt} - 2\nu_{rz}\nu_{zt}\nu_{tr})$$

and

E_r - Young's modulus in the radial (r) direction

E_z - Young's modulus in the axial (z) direction

E_t - Young's modulus in the tangential (t) direction

G_{rz} - Modulus of rigidity between the r and z direction

ν_{zt} - Poisson's ratio of t strain to z strain for a z load

ν_{rz} - Poisson's ratio of z strain to r strain for a r load

ν_{rt} - Poisson's ratio of t strain to r strain for a r load

ν_{tz} - Poisson's ratio of z strain to t strain for a t load

ν_{tr} - Poisson's ratio of r strain to t strain for a t load

ν_{zr} - Poisson's ratio of r strain to z strain for a z load

Given the ν_{ij} Poisson's ratio, the ν_{ji} ratio is easily determined by

$$\nu_{ji} = \left(\frac{E_{ji}}{E_{ij}}\right) \nu_{ij} \tag{9}$$

The strain tensor is determined from the displacements by the relationship

$$\{\varepsilon\} = \begin{bmatrix} \partial/\partial r & 0 \\ 0 & \partial/\partial z \\ 1/r & 0 \\ \partial/\partial z & \partial/\partial r \end{bmatrix} \{u\} \tag{10}$$

where r - radial coordinate

z - axial coordinate

The displacements and displacement derivatives in Eq. 10 are related to the natural coordinate system through the inverse Jacobian matrix. Using the inverse Jacobian matrix, the strain tensor in term of natural coordinates is written as

$$\{\varepsilon\} = \begin{bmatrix} (J^{\star}_{11}\partial/\partial\xi + J^{\star}_{12}\partial/\partial\eta) & 0 \\ 0 & (J^{\star}_{21}\partial/\partial\xi + J^{\star}_{22}\partial/\partial\eta) \\ 1/r & 0 \\ (J^{\star}_{21}\partial/\partial\xi + J^{\star}_{22}\partial/\partial\eta) & (J^{\star}_{11}\partial/\partial\xi + J^{\star}_{12}\partial/\partial\eta) \end{bmatrix} \{u\} \tag{11}$$

where $J^{\star}_{ij}$ - term of the inverse Jacobian matrix

Using Eq. 5, Eq. 11 is rewritten in matrix form as

$$\{\varepsilon\} = [B]\{d\} \tag{12}$$

where [B] - matrix of strain shape functions

The potential energy integral can now be written in terms of Eq. 7 and Eq. 12 as

$$I^e = \frac{1}{2} \int_{vol} \{d\}^t [B]^t [D][B]\{d\}\ dvol \tag{13}$$

Equation 13 is the potential energy for only one element. The total potential energy is found by summing all the element contributions along with the potential of any nodal loads.

$$I = \sum_{n=1}^{m} \frac{1}{2} \int_{vol} \{d\}^t [B]^t [D][B]\{d\}\ dvol + P.E. \tag{14}$$

where m - number of elements in the mesh

P.E. - potential of external loads

Equating the first variation with zero and assuming one radian of tangential integration, the total potential energy expression in natural coordinates becomes

$$\left[\sum_{n=1}^{m} \int_{-1}^{1}\int_{-1}^{1} [B]^t[D][B]r(\det J)\, d\xi d\eta\right]\{d\} = -\{F\} \tag{15}$$

where $\{F\}$ - vector of external forces

Comparing Eq. 15 with Eq. 2, the element stiffness matrix is defined by the area integral

$$[K^e] = \int_{-1}^{1}\int_{-1}^{1} [B]^t[D][B]r(\det J)\, d\xi d\eta \tag{16}$$

where $[K^e]$ - Stiffness matrix of element e

The vector of nodal forces in Eq. 15 is broken down into the following four integrals; (1) nodal forces due to initial stresses, (2) nodal forces due to initial strains, (3) nodal forces due to body forces and (4) nodal forces due to surface tractions. In matrix notation these integrals are

$$\{F\} = \int_{vol} [B]^t\{\sigma_o\}\, dvol - \int_{vol} [B]^t[D]\{\varepsilon_o\}\, dvol - \tag{17}$$

$$- \int_{vol} [N]^t\{b\}\, dvol - \int_{area} [N]^t\{t\}\, darea$$

where $\{\sigma_o\}$ - vector of element initial stresses

$\{\varepsilon_o\}$ - vector of element initial strains

$\{b\}$ - vector of element body forces

$\{t\}$ - vector of surface tractions

$[N]$ - matrix of shape functions

The body forces and surface tractions are assumed to be zero, as are the forces due to initial strains. The nodal forces due to initial stresses are non-zero because the winding tension is taken to be an initial stress in the fiber direction. Also, the nodal loads caused by a change in temperature are treated as initial stresses.

Assuming one radian of tangential integration, the force integral written in natural coordinates becomes

$$\{F\} = - \int_{-1}^{1} \int_{-1}^{1} [B]^t \{\sigma_o\} r (\det J) \, d\xi d\eta \tag{18}$$

Generally, the integrands in Eq. 16 and Eq. 18 are complicated polynomials in ξ and η that must be evaluated numerically. The numerical scheme used to evaluate Eqs. 16 and 18 is two point Gauss quadrature. The governing equation for two point Gauss quadrature is

$$\int_{-1}^{1} \int_{-1}^{1} f(\xi,\eta) \, d\xi d\eta = \sum_{i=1}^{2} \sum_{j=1}^{2} H_i H_j f(\xi_i,\eta_j) \tag{19}$$

where $f(\xi,\eta)$ - function of ξ and η to be integrated

$f(\xi_i,\eta_j)$ - value of function at the sampling points

H_i and H_j - weighting coefficients

The two point integration is reduced to one point integration for the case where one side of a quadrilateral element is collapsed to form a triangular element. The reduced integration is intended to make the triangular element less sensitive to the numbering scheme used to define the element.

This completes the basic formulation of the finite-element method as presented in reference 1. The details of the computer implementation and adaptation to the simulation of the filament winding process follow.

4 FINITE-ELEMENT IMPLEMENTATION

4.1 INTRODUCTION

This chapter focuses on the computer implementation of the concepts presented in chapter 2 as well as how the concepts have been modified to suit the special geometric and elastic behavior characteristics of a filament wound structure. The chapter is divided into six topical sections; (1) discussion of WACSAFE program operation, (2) element material states, (3) orthotropic considerations, (4) layered element theory, (5) special stress-strain computations and (6) thermal stress implementation.

4.2 WACSAFE PROGRAM OPERATION

The basic operation of the finite-element program WACSAFE is summarized in the flow chart shown in Fig. 3. Figure 3 is not meant to be an exact graphical representation of the program logic, but is intended to aid in the understanding of the overall program structure. Used in conjunction with a listing of the program, the more intricate logic structures in the program can be examined if desired. The following paragraphs describe in greater detail each of the blocks in Fig. 3.

The column headings in Fig. 3 describe the collection of subroutines that perform the functions listed in the blocks below each.

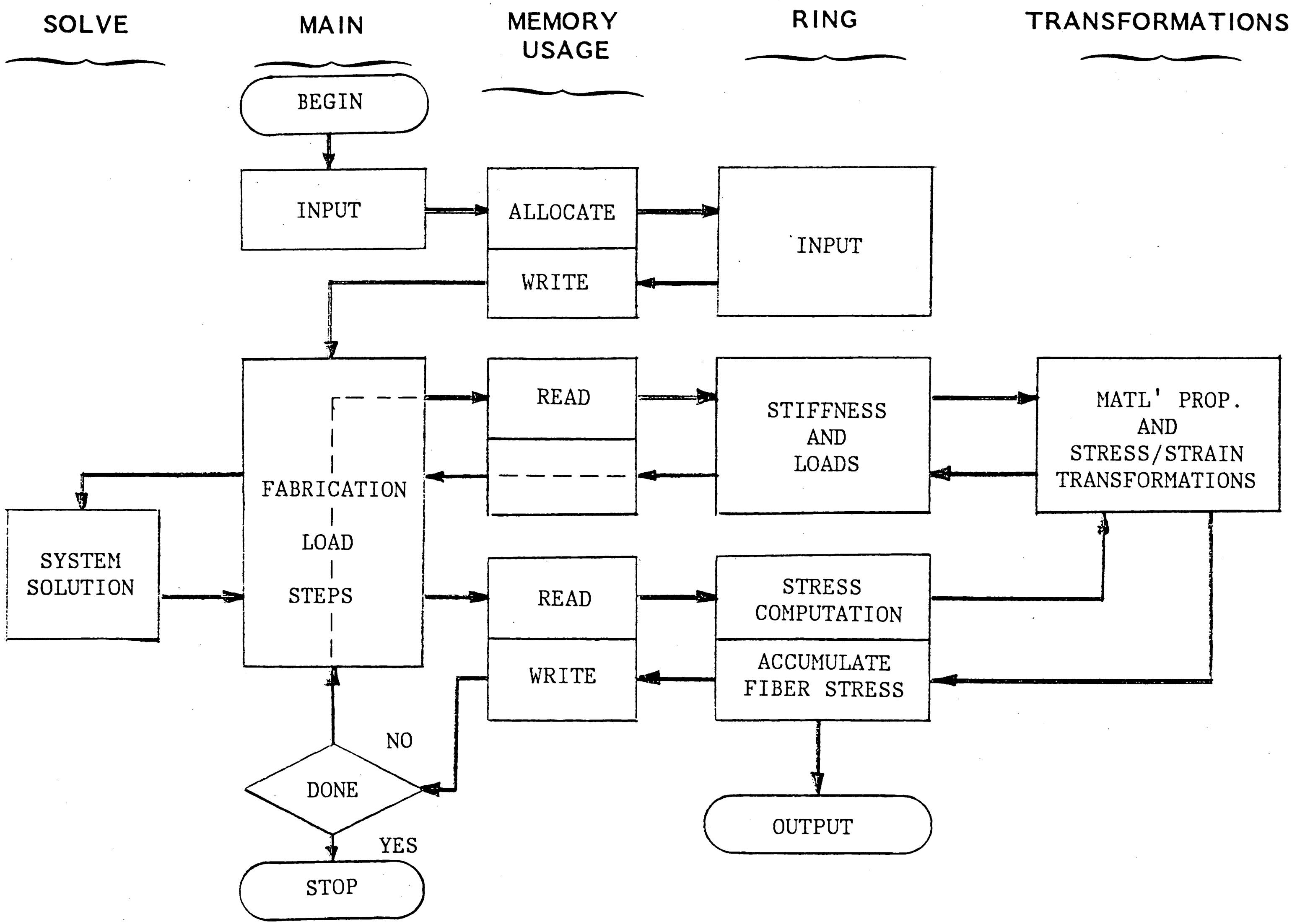

Figure 3. Flow chart of WACSAFE finite-element program

The program begins at the top of the main program with the input of various control information such as the number of nodes in the model, the number of element groups, the number of winding and thermal load steps to be performed, and whether or not a full output listing is desired. Temporary memory space is set aside and the nodal data read. If thermal steps are to be performed, the nodal temperatures are also read for all thermal steps. The program then reads additional control information such as the number and type of elements and number of material sets.

Moving into the memory usage column, the program allocates memory space for the material and element data. Two sets of material data are required, one set for uncured properties and a second for cured properties. This data is read in the input block of the ring column (subroutine) and then written to a disk file (along with the nodal data) as the program returns to the main program. This data is recalled periodically during execution as needed. The use of out-of-core data storage during execution increases the maximum size problem that can be solved on any given computer. However, this method does sacrifice execution speed.

The blocks in the ring column are three distinct branches of a single subroutine, hence the reference in the preceding paragraph. The function of each of these branches is well documented by the block label (Input, Stiffness and Stress).

After the initial data write with the program flow returned to the main program, the program begins looping over the number of fabrication steps specified. First, the geometry and load data is reread from the disk file and placed into memory. The global stiffness matrix is then assembled from the individual element stiffness matrices and is efficiently stored in a skyline fashion. The global force vector is assembled similarly from external loads or internal loads due to an initial stress in model. The material property transformations are utilized here to handle the orthotropic composite elements.

The program flows back through the stiffness block to the main program where a node sequence solver is employed to solve for the nodal displacements of all the degrees of freedom present. Since the model data is destroyed during the solution of the system, the model data must be reread from disk file. This data along with the displacement profile is then used to compute the stress-strain state in the model. The stresses or strains are transformed into fiber coordinates and the stress increment computed in this load step is added to the accumulated fiber direction stress. If the output suppression flag is disabled, this stress increment and accumulated stress is output to a listing file; otherwise, only the last increment and final accumulated fiber stress is output. The stress data is then written to a disk file.

If the current load step is the final fabrication step, be it a winding or thermal step, the program terminates; otherwise, a new load step is initiated and the process repeats.

One important programming feature of WACSAFE that should be included in any program outline is the memory allocation scheme used. In WACSAFE, all program variables (including multi-dimensional arrays) are stored in a one dimensional [A] array. A list of pointers track the end of one variable and the beginning of another. The large global stiffness matrix is efficiently stored in the [A] array in a skyline fashion where only those terms below the skyline are retained.

The one dimensional [A] array scheme allows the maximum in-core memory allocation to be increased or decreased simply by modifying the dimension statement for the [A] array and the maximum storage variable. For a problem of approximately 1500 nodes and 1300 elements, the necessary program lines would be

```
COMMON A(500000)
MTOT = 500000
```

For a more detailed discussion of this storage scheme, the reader is referred to Bathe [11].

4.3 ELEMENT MATERIAL STATES

In this section the following topics are discussed; (1) the simulation of material addition by specifying an IOFFON number and (2) the different material states that an element can assume. These features of WACSAFE are monitored by the assignment of element material states. An element material state is defined by the values of three program flags; NORM, NSTRS and JOFF. An element can assume four different material states while uncured but only one material state after cure.

All winding load steps are assumed to occur with uncured material. Thus, during winding an element must assume one of the four available uncured material states. On the other hand, during a thermal load step, the material can be uncured as in the heating cycle, or cured as in the cooling cycle. Even though both winding and thermal load steps can be performed with uncured material, the program is design with the restriction that winding and curing never overlap. This eliminates the possibility of simulating the layer-by-layer curing process discussed by Tarnopol'skii, et. al., [5]. However, this limitation did not adversely affect this study because the test cases considered do not use layer-by-layer curing.

The turning on of elements that are off, to simulate material addition in the winding stage, is accomplished by specifying the load step (IOFFON number) during which each element will be added to the model. Prior to this load step, the element state is considered to be off and the material stiffness matrix values are reduced by a factor of 10^7. The elemental stiffness matrix for an element in this state has almost no effect on the assembled structural stiffness matrix yet does not cause numerical difficulties such as singularities or illconditioning. Also, for an element in this material state, the stress computation, stress accumulation, stress output and write to disk blocks in Fig. 3 are skipped. This material state corresponds to line one of Table 1.

When the IOFFON number for an element is equal to the current program load step, the element is turning on and corresponds to the second line of Table 1. The element stiffness is calculated by setting the fiber direction modulus equal to the modulus in the first transverse (resin) direction. Reduced fiber properties are used for an element in this material state because the full properties would allow the element turning on to support much of the initial stress used to simulate the winding tension instead of having the underlying composite layers support the stress load. The nodal loads resulting from the initial stress in this

Table 1. Program variables that define material state.

MATERIAL STATE DESCRIPTION	STIFFNESS PASS			NODAL LOADS CALCULATION			STRESS PASS	
	JOFF	NORM	NSTRS	JOFF	NORM	NSTRS	NORM	NSTRS
** OFF **								
ISOTROPIC	1	1	0	*	*	*	*	*
COMPOSITE	1	1	0	*	*	*	*	*
* TURNING ON *								
ISOTROPIC	1	2	0	0	0	0	*	*
COMPOSITE	1	2	0	0	0	0	*	*
** ON ** (TENSION)								
ISOTROPIC	1	0	0	0	0	0	0	0
COMPOSITE	1	0	0	0	0	0	0	0
** ON ** (COMPRESSION)								
ISOTROPIC	1	0	1	0	0	0	0	1
COMPOSITE	1	0	1	0	0	0	0	1

element are calculated using Eq. 12, in which the $[B^t]$ matrix is computed using the full material properties.

These two material states are unique to the winding simulation and therefore are unavailable after curing has occurred. Also, since there is no overlapping of winding steps and thermal steps, an element during a thermal step may never assume one of these two material states.

In all elements that are already turned on, one of two remaining material states can be assumed. If the accumulated stress in the fiber direction is tensile, the element stiffness is computed using the full element properties. However, elements that have lost all of their initial winding tension and exhibit compressive accumulated stress in the fiber direction, are made isotropic by reducing the fiber direction properties to the transverse (resin) properties. This is done because fibers with only the wet resin material for lateral support will buckle under compressive loads. Recalling that a buckling structure will support virtually no axial load suggests that the element stiffness will be dominated by the resin properties. Hence the aforementioned reduction. This has no effect on the mandrel or any other isotropic elements in the model since the properties are equal in every direction. These two states correspond to the third and fourth lines of Table 1 respectively.

An exception to the rule above occurs when an element that has already cured is loaded in compression. In this case, the element properties are not reduced because the fibers, frozen in the resin matrix, are very much less likely to buckle under load.

The states of the first fifty elements can be followed by enabling the tracing option of WACSAFE. This option makes an entry in a state table every time the material stiffness subroutine (MATSTF) is accessed. The MATSTF subroutine is accessed during; calculation of element stiffness matrices, calculation of nodal loads from initial stresses and calculation of element stresses. The state tables can be output by disabling the output suppression flag.

4.4 ORTHOTROPIC CONSIDERATIONS

A filament wound structure consists of overlapping layers of composite material, each having a specified wrap angle. In a finite-element model of such a structure, each element will have associated with it a fiber angle that gives the direction of fibers passing through the volume bounded by the element. In WACSAFE, the fiber angle is measured relative to a line of latitude drawn through the element centroid. The elements in the dome portion of the structure will also have an inclination or polar orientation angle associated with them. These two angles are referred to as BETA and SETA respectively, and are illustrated in Fig. 4.

It is important to note that several references are made in this section to layered elements and the assumptions associated with them. While the full discussion of this topic is delayed until the next section, it is sufficient at this time to know that a layered element consists of two bands of fiber material, one having the wrap angle BETA and the other having the opposite angle of -BETA.

The element's local coordinate system is the fiber or 1-2-3 system. The 1-2-3 coordinate system is a right hand system with the 1-axis par-

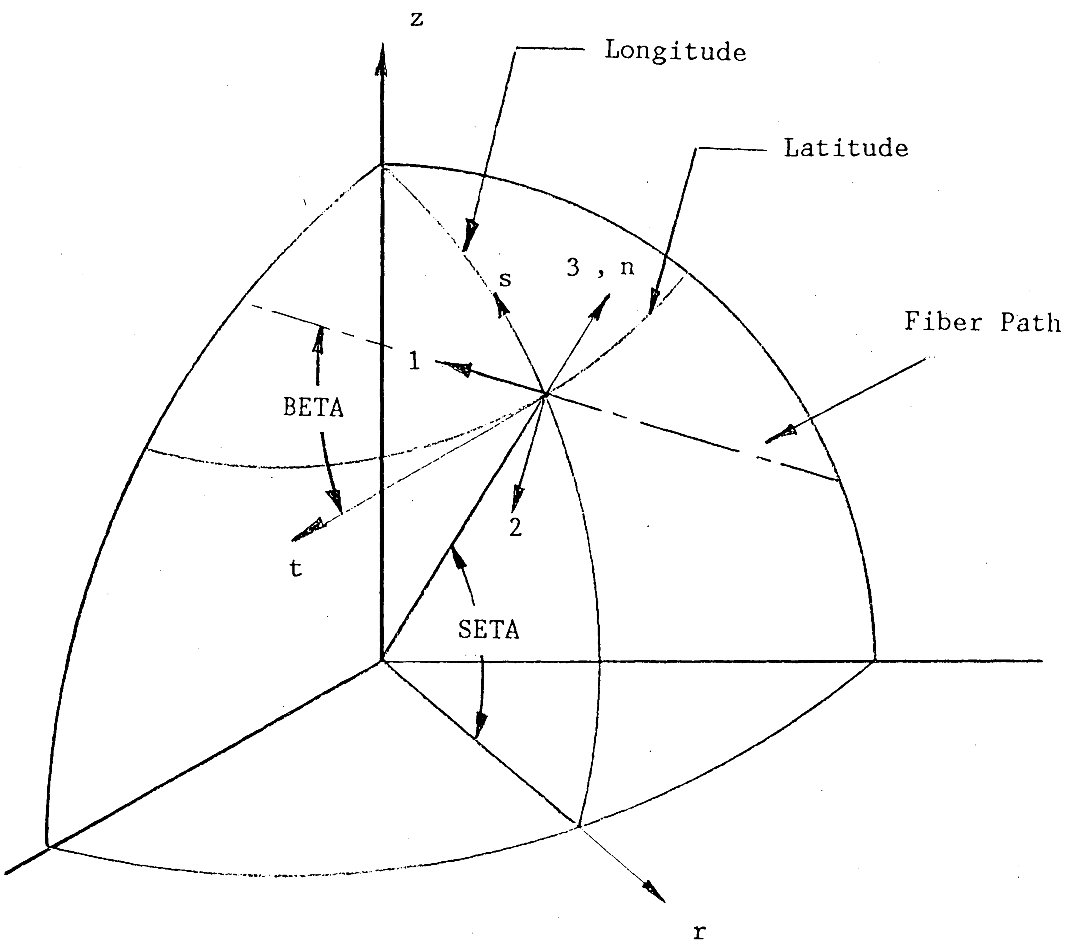

Taken from Ref.[1]

Figure 4. Three dimensional view of angles BETA and SETA

allel to the fiber path and the 2- and 3-axes tangent and outward normal to the structure's surface. Figure 4 illustrates this convention.

The axisymmetric finite-element analysis is carried out in the r-z-t or global coordinate system. The material properties are defined in the fiber coordinate system. Therefore, the material properties must be transformed. In addition, the initial stresses due to winding and curing are defined in the fiber coordinate system and also must be transformed. Lastly, the stresses are computed in the global system but are output in the fiber system so they too must be transformed. This section deals with these transformations and is divided into three subsections; (1) fiber to global material transformations, (2) fiber to global stress-strain transformations and (3) global to fiber stress-strain transformations.

The 3-space master transformation matrix from reference 13 (Fig. 5) is used as the basis for the three transformations. In the case of the stress-strain transformations, the individual matrices were derived from the matrix in Fig. 5 by substituting the specified rotation angles into the master matrix and eliminating terms containing sines and cosines of 90°. The implementation of the material transformation utilizes the tabulated equations in reference 13.

The material property transformation is accomplished by performing two fourth order tensor transformations. The matrix equation

$$[D'] = [T_m]^t \, [D] \, [T_m] \tag{20}$$

where [D] - matrix of material properties (stiffness)

[D'] - matrix of transformed material properties

$$[T_m] = \begin{bmatrix} N^2 & M^2 & 0 & 0 & 0 & 2MN \\ M^2 & N^2 & 0 & 0 & 0 & -2MN \\ 0 & 0 & 1 & 0 & 0 & 0 \\ 0 & 0 & 0 & N & -M & 0 \\ 0 & 0 & 0 & M & N & 0 \\ -MN & MN & 0 & 0 & 0 & (N^2 - M^2) \end{bmatrix}$$

Where M - Sine of the rotation angle

N - Cosine of the rotation angle

Figure 5. Master transformation matrix

$[T_m]$ - second order transformation matrix

$[T_m]^t$ - transposed second order transformation matrix

gives the mathematical relationship which describes the material transformations. For a proper rotation through a positive angle, the master transformation matrix is used in Eq. 20.

The material properties are first rotated about the 3-axis to the s-t-n coordinate system shown in Fig. 6(a). The 3- and n-axes are coincident axes and the rotation angle is BETA-90. In this transformation, the existence of shear coupling is neglected due to the layered element assumption discussed in the following section.

Next, the s-t-n system is permuted to a n-s-t system. The second transformation is a rotation about the t-axis to the r-z-t coordinate system shown in Fig. 6(b). The rotation angle for the second transformation is (-SETA). The shear coupling terms are neglected during this transformation even though both layers making up an element are rotated through the same angle.

In WACSAFE, the material transformation is performed in its own subroutine named TRAN. The equations used in TRAN were obtained from Tsai, [13] who performed and tabulated symbolically the matrix multiplications specified in Eq. 20. In Eq. 20, the material property matrix can be either the stiffness or the compliance matrix. For uncured computations, the compliance is transformed while for cured computations, the stiffness is transformed.

The stress-strain transformations, both to and from fiber coordinates, are accomplished by performing two second order tensor transf-

a) Beta - view along spherical radius or n- and 3- axis

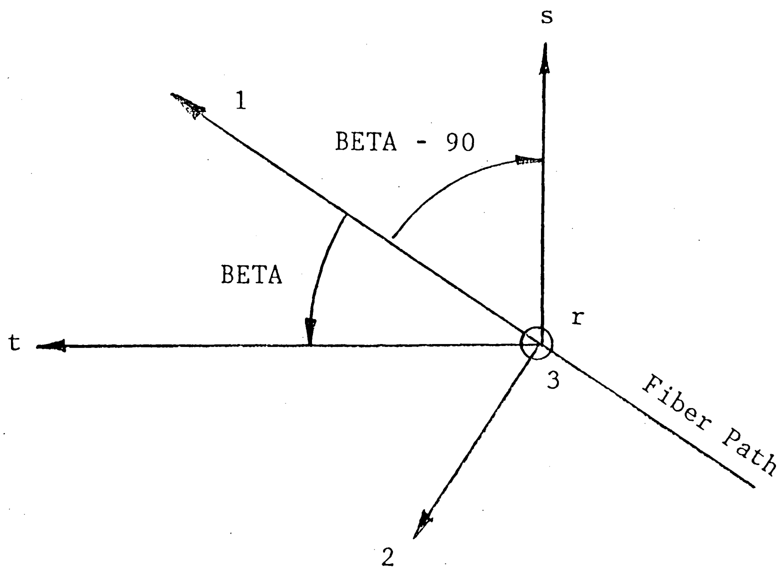

b) Seta - view in tangential direction along t- axis

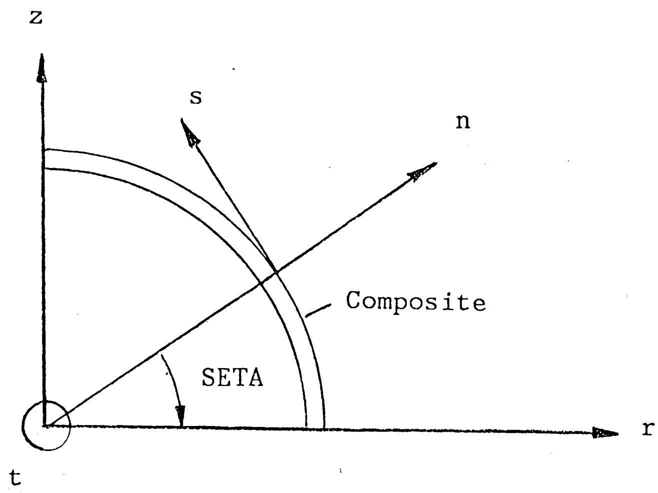

* Taken from Ref.[1]

Figure 6. Transformation angles: (a) fiber angle BETA, (b) polar orientation angle SETA

ormations. Second order transformation matrices are required because stress and strain are second order tensor quantities. Rather then duplicate material by discussing both stress and strain transformations, only the stress transformations are presented. However, the transformations are equally valid for transforming the tensor strains.

The fiber to global stress transformation is carried out through the same angles as the material transformation. The basic matrix equation describing the transformation is

$$\{\sigma_o\} = [T_i]\{\sigma_o'\} \tag{21}$$

where $\{\sigma_o\}$ - tensor of initial stresses

$\{\sigma_o'\}$ - tensor of transformed initial stresses

$[T_i]$ - second order transformation matrix, i = 1-4

The matrix in Fig. 7(a) is used to perform the 1-2-3 to s-t-n transformation. The s-t-n system is then permuted as before to a n-s-t system. Next, the n-s-t to r-z-t transformation is performed by using the matrix in Fig. 7(b).

Figure 7(a) differs from the transformation matrix given in reference 4 by the (6,6) term. Reference 4 gives the (6,6) term as $M^2 - N^2$ when the term should be $N^2 - M^2$. This correction was implemented and validated. The corrected matrix in Fig. 7(a) is consistent with the master transformation matrix. The transformation is performed in the FTRAN subroutine.

a)

$$[T_1] = \begin{bmatrix} M^2 & N^2 & 0 & 0 & 0 & -2MN \\ N^2 & M^2 & 0 & 0 & 0 & 2MN \\ 0 & 0 & 1 & 0 & 0 & 0 \\ 0 & 0 & 0 & M & N & 0 \\ 0 & 0 & 0 & -N & M & 0 \\ MN & -MN & 0 & 0 & 0 & (M^2 - N^2) \end{bmatrix}$$

b)

$$[T_2] = \begin{bmatrix} N^2 & M^2 & 0 & 0 & 0 & -2MN \\ M^2 & N^2 & 0 & 0 & 0 & 2MN \\ 0 & 0 & 1 & 0 & 0 & 0 \\ 0 & 0 & 0 & N & M & 0 \\ 0 & 0 & 0 & -M & N & 0 \\ MN & -MN & 0 & 0 & 0 & (N^2 - M^2) \end{bmatrix}$$

Where M - Sine of the rotation angle

N - Cosine of the rotation angle

Figure 7. Stress transformation matrices: (a) 1-2-3 to s-t-n transformation matrix (b) n-s-t to r-z-t transformation matrix.

a)

$$[T_3] = \begin{bmatrix} N^2 & M^2 & 0 & 0 & 0 & 2MN \\ M^2 & N^2 & 0 & 0 & 0 & -2MN \\ 0 & 0 & 1 & 0 & 0 & 0 \\ 0 & 0 & 0 & N & -M & 0 \\ 0 & 0 & 0 & M & N & 0 \\ -MN & MN & 0 & 0 & 0 & (N^2 - M^2) \end{bmatrix}$$

b)

$$[T_4] = \begin{bmatrix} M^2 & N^2 & 0 & 0 & 0 & 2MN \\ N^2 & M^2 & 0 & 0 & 0 & -2MN \\ 0 & 0 & 1 & 0 & 0 & 0 \\ 0 & 0 & 0 & M & -N & 0 \\ 0 & 0 & 0 & N & M & 0 \\ -MN & MN & 0 & 0 & 0 & (M^2 - N^2) \end{bmatrix}$$

Where M - Sine of the rotation angle

N - Cosine of the rotation angle

Figure 8. Stress transformation matrices: (a) r-z-t to n-s-t transformation matrix (b) s-t-n to 1-2-3 transformation matrix.

In the FTRAN subroutine, the τ_{st} term is set equal to zero after the first transformation to reflect the layered nature of the composite elements.

Since the global to fiber stress transformation is the inverse of the fiber to global transformation, the process is very similar and the governing equation is the same as Eq. 21. However, the two matrices shown in Fig. 8(a) and 8(b) are derived by substituting rotation angles of the opposite sign into the master matrix. This transformation is performed in the STRAN subroutine. Also, the τ_{st} and τ_{tn} terms are set equal to zero to remain consistent with the layered element and axisymmetric assumptions.

Both FTRAN and STRAN subroutines can be used to transform strains between fiber and global coordinates if care is taken to use the tensor strain rather than engineering strain in the subroutine calls.

4.5 LAYERED ELEMENT THEORY

The winding process covers the structure with bands of fiber that are applied with a specified wrap angle (BETA). The geometry of a complete winding circuit dictates that every point on the structure will be covered with two bands of fiber. The two bands will have opposite wrap angles at the point where they cross. This is illustrated in Fig. 9. The finite-element model assumes that a single element is composed of both +/- fiber bands. However, only the positive band is considered in the stiffness and stress computations. The reasoning behind this technique follows.

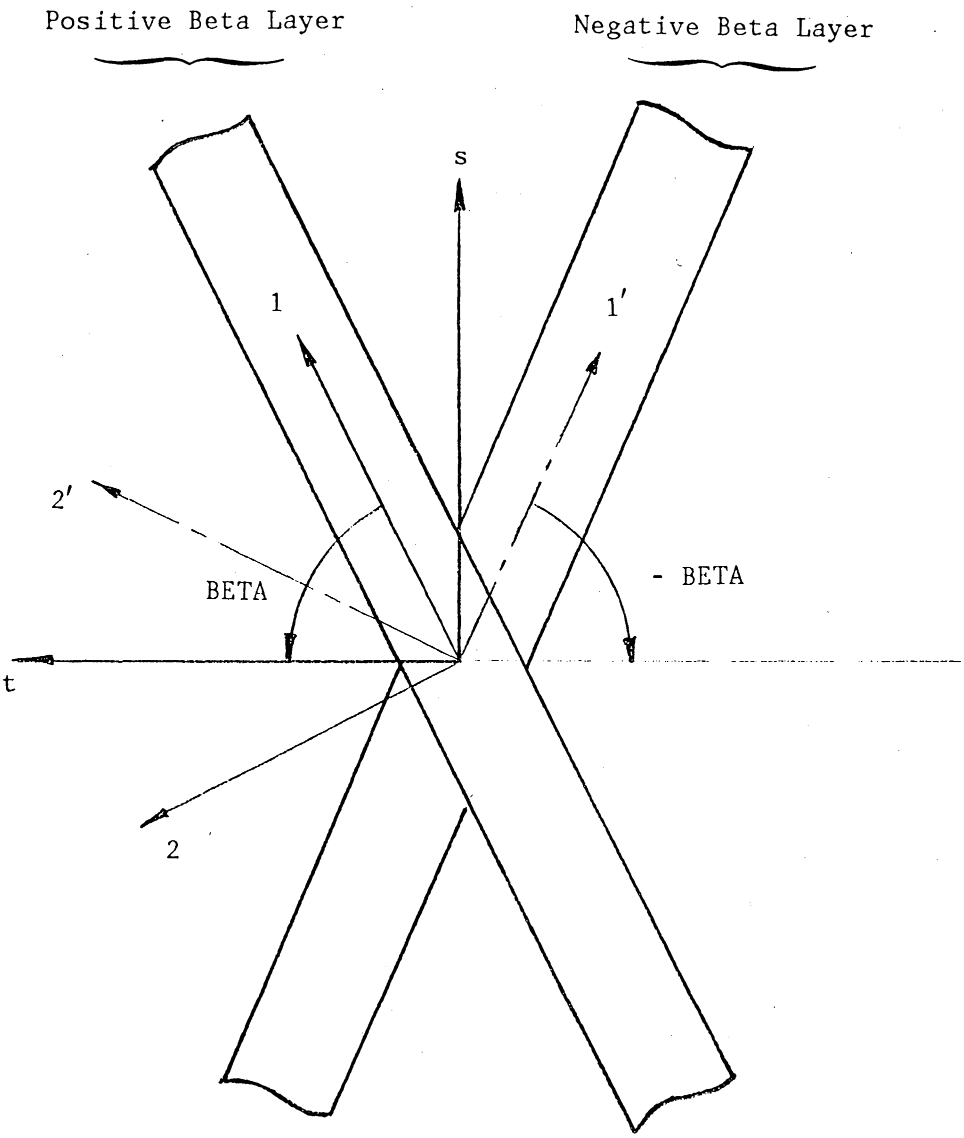

Figure 9. Crossing of fiber bands with opposite wrap angles BETA.

The symmetric orthotropic stiffness matrices of two layers consisting of entirely positive or entirely negative fiber bands, when transformed from the 1-2-3 to the s-t-n coordinate systems, will differ only in the (1,6), (2,6) and (3,6) terms (the shear coupling terms). These terms will have the same magnitudes but opposite signs. The change of sign occurs because only these terms in the transformation equations [13] have odd powers of sin(BETA). The layered element theory utilizes this symmetry to combine the two bands into one.

If the material is cured and the bands are very thin, then it is safe to assume that the bands are rigidly bonded to each other, as in classical lamination theory, and that the strain state in both bands is equal.

The average stress state in the plus and minus bands is expressed by averaging their respective stress vectors.

$$\frac{\{\sigma^{+}\} + \{\sigma^{-}\}}{2} = \frac{[D^{+}]\{\varepsilon^{+}\}}{2} + \frac{[D^{-}]\{\varepsilon^{-}\}}{2} \tag{22}$$

where $\{\sigma^{+}\}$ - stress vector for + BETA band

$\{\sigma^{-}\}$ - stress vector for - BETA band

$\{\varepsilon^{+}\}$ - strain vector for + BETA band

$\{\varepsilon^{-}\}$ - strain vector for - BETA band

$[D^{+}]$ - Orthotropic stiffness matrix for + BETA band

$[D^{-}]$ - Orthotropic stiffness matrix for - BETA band

Because the strain state in both bands is equal, the strain vector can be factored out of Eq. 22 and designated simply as $\{\varepsilon\}$. The average stress in the two layers is now

$$\frac{\{\sigma^+\} + \{\sigma^-\}}{2} = \left\{\frac{[D^+] + [D^-]}{2}\right\}\{\varepsilon\} \tag{23}$$

The quantity on the left hand side of Eq. 23 is the defined as the stress in the layered element. Therefore, the stiffness matrix for the layered element (quantity in brackets) is the stiffness matrix of either the plus or minus layer with the shear coupling terms deleted. These terms are zero because for the plus and minus layers, the shear coupling terms are of equal magnitude but opposite sign and therefore sum to zero. A consequence of this technique is that the average τ_{st} stresses in the layered element will be zero even though each layer will have non-zero shears. At this time, no attempt is made to recover these shears.

In the case of uncured material, the stresses are assumed to be equal in each band because each band supports the same load vector independently without a bond existing between the crossing bands. This allows a scissoring action to occur in the uncured layered element (Fig. 10). The stress-strain development for the uncured layered element is similar to that for the cured element, except that the equal stresses in each band are factored out and the element compliances combined by averaging the strains.

$$\frac{\{\varepsilon^+\} + \{\varepsilon^-\}}{2} = \left\{\frac{[C^+] + [C^-]}{2}\right\}\{\sigma\} \tag{24}$$

where $[C^+]$ - Orthotropic compliance matrix for + BETA band

$[C^-]$ - Orthotropic compliance matrix for - BETA band

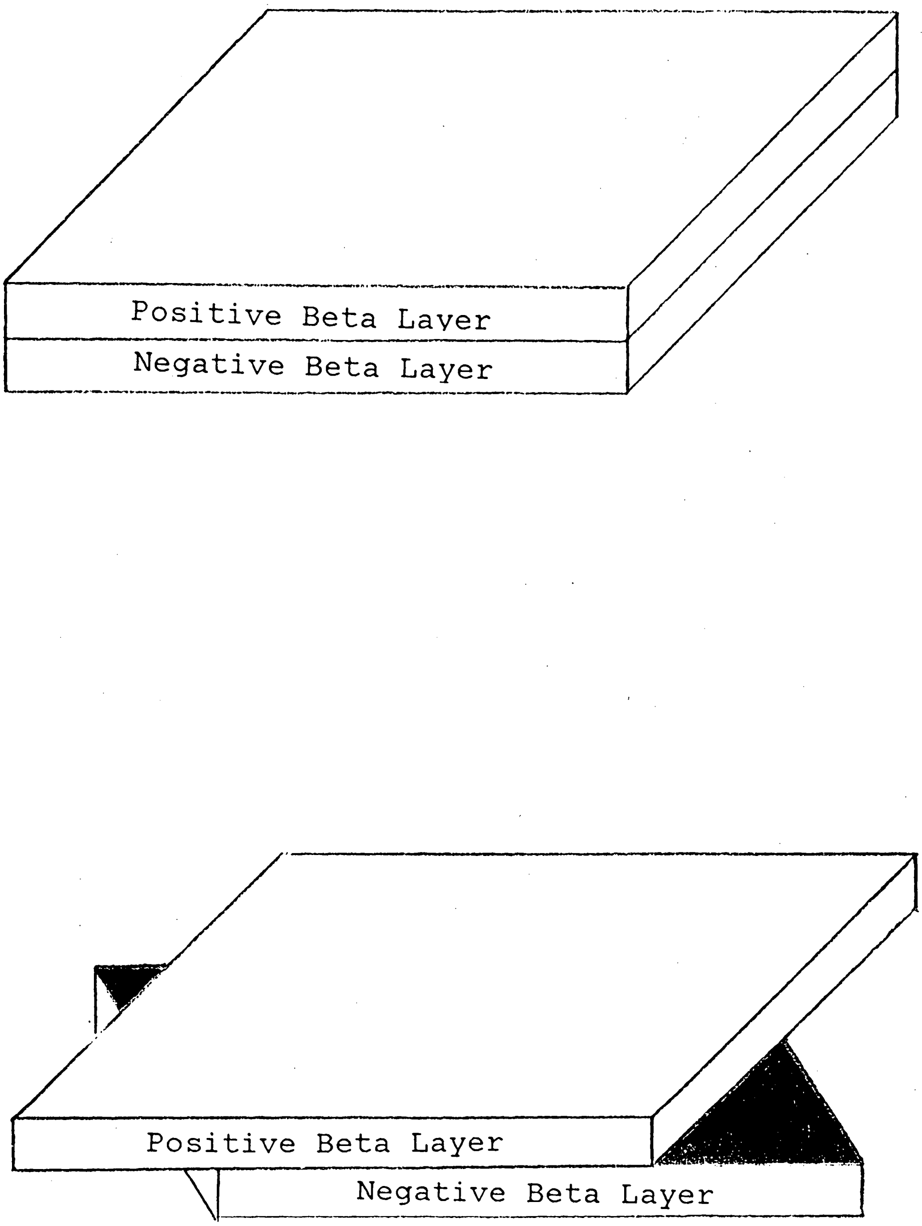

Figure 10. Scissoring of uncured fiber layers.

The bracketed quantity is the compliance matrix of the layered element, and is equal to the compliance matrix of the plus layer with the shear coupling terms deleted. Inverting the combined compliance gives the material stiffness matrix required for finite-element computations.

The two methods for computing the material stiffness matrix will yield the same result for isotropic materials such as the mandrel elements, however, the elimination of the shear coupling terms in either the stiffness or compliance matrices will produce different results for the oriented composite elements.

Another consequence of the layered element assumption is that that special care must be exercised when computing the layered element stresses and strains. This topic is discussed in the next section.

4.6 STRESS-STRAIN COMPUTATIONS

The manner in which stresses and strains are computed in WACSAFE distinguish it from other orthotropic finite-element programs. Specifically, the transformations to and from fiber coordinates are dependent on the stage of fabrication that is being considered. This dependence is a result of the layered element assumption.

In the uncured winding stage the two bands making up a layered element are theoretically free to shear in a scissor fashion (Fig. 10). Although continuity of element displacements prevents this type of motion, the stiffness and stress computations make an approximation to this condition. Since the bands are free from interaction and they each support half the applied load, the stress state is the same in each band.

This is the exact stress state computed in the global coordinate system. Then, to get the stresses in fiber coordinates, simply transform the stress vector through the angle BETA. Uncured composite computations are performed during the winding steps and also during the heating cycle.

In contrast, after curing the bands are considered to be perfectly bonded to one another. Therefore, the strains in each band are equal. Although the average global shear stresses are zero, the shear stresses in each layer are non-zero. Without knowing the shear stress magnitudes, the shear transformation cannot be done. Therefore, to obtain the correct layer stresses, the strains are transformed on cured laminates as in classical lamination theory. After the strains are transformed to fiber coordinates, the correct fiber coordinate stresses are computed using the material stiffness matrix in fiber coordinates. Cured stress computations are performed during the cool-down cycle of the cure stage.

4.7 THERMAL STRESS IMPLEMENTATION

The addition of thermal stress capability to WACSAFE follows the standard implementation outlined by Zienkiewicz [8]. In this section, the calculation of nodal loads due to initial thermal stress, which was mentioned in section 2.2, is discussed in greater detail. The calculation of mechanical stresses from the nodal displacements and the manner in which the temperatures are processed are also discussed in this section.

The nodal loads are computed from the initial stress by first computing the thermal free strain in each element.

$$\{\varepsilon^{th}\} = \{\alpha\}\ (T - T_o) \tag{25}$$

where
- $\{\varepsilon^{th}\}$ - vector of thermal free strains
- $\{\alpha\}$ - vector of thermal expansion coefficients
- T - present temperature
- T_o - previous temperature

The vector of thermal expansion coefficients is defined in the fiber coordinate system. Therefore, the thermal strain vector computed from Eq. 25 is with respect to this coordinate system. If the element is uncured, the initial thermal stresses are computed and then transformed into the global system. If the element is cured, the initial thermal strains are first transformed into the global coordinate system and the global initial thermal stress computed. This is consistent with the layered element assumption previously discussed.

Next, the nodal loads are computed using Eq. 16 and the global force vector assembled. The stiffness matrix is then decomposed and solved yielding the nodal displacements.

In the case of totally unconstrained thermal expansion (contraction), the stresses generated by the nodal displacements are equal to zero. Therefore, the stress-strain state computed from the nodal displacements must have the thermal free stress-strains removed to obtain the actual mechanical stress-strain state in the element.

If the element material is uncured, the model global stresses are first computed and then transformed to the fiber coordinate system. The initial thermal stress in fiber coordinates is then computed and subtracted as in Eq. 26.

$$\{\sigma_m\} = \{\sigma'\} - [D]\ \{\varepsilon^{th}\} \tag{26}$$

where $\{\sigma_m\}$ - vector of mechanical stresses in fiber coordinate system

$\{\sigma'\}$ - transformed vector of model global stresses

$[D]$ - material stiffness matrix in fiber coordinate system

If the element is cured the model global strains are computed and transformed to fiber coordinates. The model stresses are then computed using the fiber coordinate material stiffness matrix and the thermal stresses subtracted as in Eq. 26. These two approaches are utilized in WACSAFE to maintain consistency with the layered element assumption.

The thermal analysis requires that the temperature at every node point in the structure be known and stored for every thermal load step considered. For large finite-element problems (number of nodes > 1000), efficient processing of the nodal temperatures is crucial. In WACSAFE, the reference temperature and nodal temperatures for all load cases are read into temporary high-speed storage and then stored on a disk file.

At any point during a thermal load step, only the present array of nodal temperatures, the previous array of average element temperatures and the change in average element temperatures are present in memory. At the beginning of a thermal load step, the new nodal temperatures are read from the disk file and the average element temperature is calculated. The change in average element temperature from the previous step is computed and then the present element temperatures are transferred to the previous step. The change in average element temperature is then used to compute the thermal strain vector.

5 MODEL PREPARATION

5.1 GENERAL INPUT REQUIREMENTS

The finite-element program WACSAFE requires a large amount of data input. The finite-element model must include the global coordinates of all the nodes and the connectivity matrix defining element boundaries. Each element must have associated with it a set of material properties, a fiber direction angle and a polar orientation angle. In addition, each element is assigned an initial stress value for the fiber winding stress and the load step during which the element is turned on. Nodal temperatures for each thermal load step must also be input if a thermal analysis is desired. For a typical problem of approximately 1000 nodes and elements, the input file will contain over 20,000 individual values. Inputting these values by hand is impractical. The user has two alternatives available; (1) generate the entire input file or (2) build up the input file from existing geometry and material files, generating only the additional data required. The existence of the TASS [14] preprocessor and the development of the WACFORM preprocessor enable the second alternative to be used.

The TASS preprocessor output provides partial geometry and material assignment files for an 18 in. (457 mm) graphite fiber reinforced filament wound bottle shown in Fig. 11. The TASS modeling effort is reduced by assuming that the structure is axisymmetric about the vertical axis and symmetric about the equatorial plane. This simplification requires that

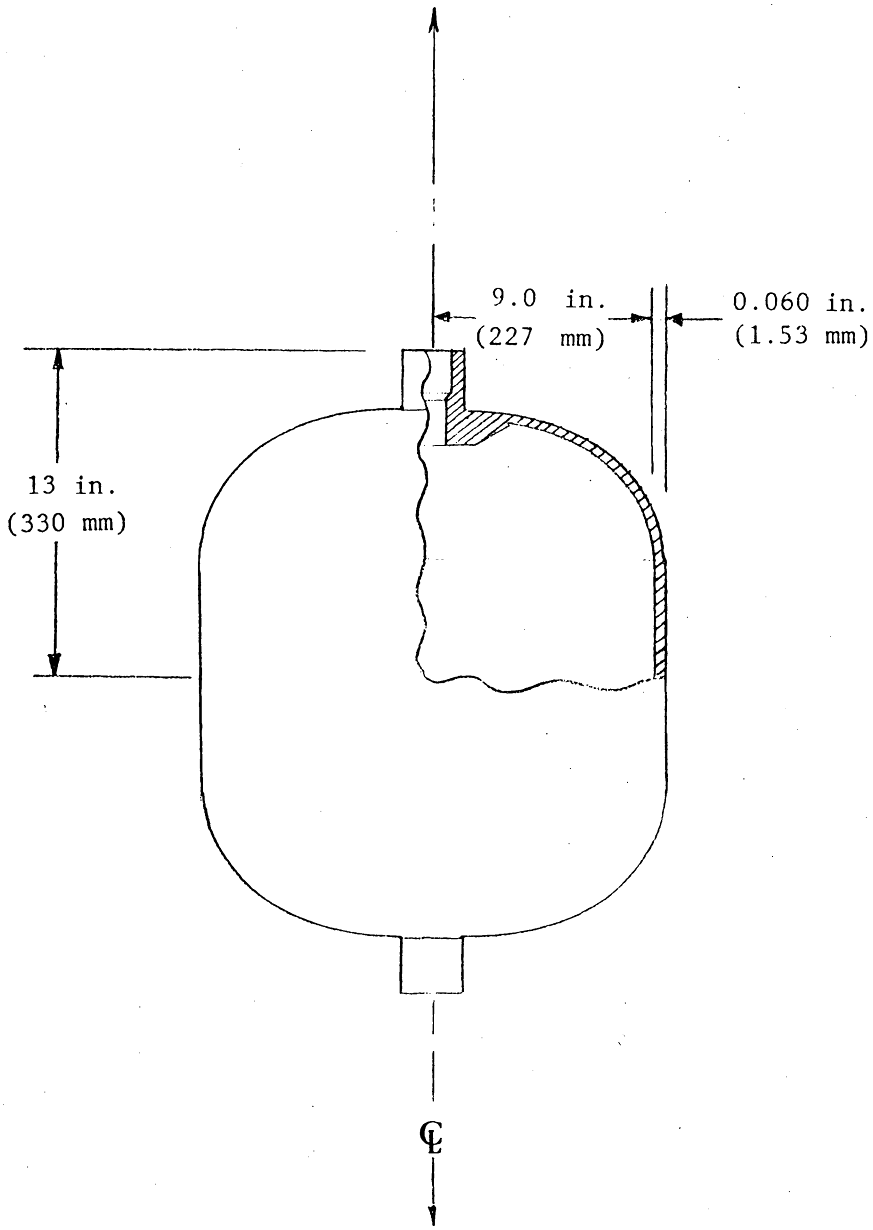

Figure 11. 18 in. (457 mm) Graphite fiber-reinforced filament wound bottle

only one quarter of an axial cross section be modeled. Additional geometry and material data, such as mandrel elements, along with boundary and fabrication data must be generated by the WACFORM preprocessor. The following sections describe in detail the TASS data and the WACFORM preprocessor used to generate the complete WACSAFE input file. Refer to the WACFORM users guide [12] for more detail on input formats.

5.2 TASS GEOMETRY

The TASS geometry file contains the nodal coordinates, element connectivities, material assignment numbers and polar orientation angles (SETA) for the composite layers and the polar boss. The TASS mesh for these two components is shown in Fig. 12. It is important to note that there are 6 composite layers and 119 radial element sections in the mesh. Figure 13 details the transition from the cylindrical wall to the dome cap while Fig. 14 is an enlargement of the polar boss region showing the termination of the composite layers.

The shaded layer of elements separating the boss from the composite layers in Fig. 14 are rubber elements. The TASS geometry file includes only those rubber elements shown. The rubber layer on the actual structure covers the entire inside surface of the structure, not just the interface between the polar boss and the composite layers. These additional rubber elements must be generated by the WACFORM preprocessor.

The global coordinate system is shown in Fig. 15 along with several major dimensions. The centerline of the bottle is the zero reference for

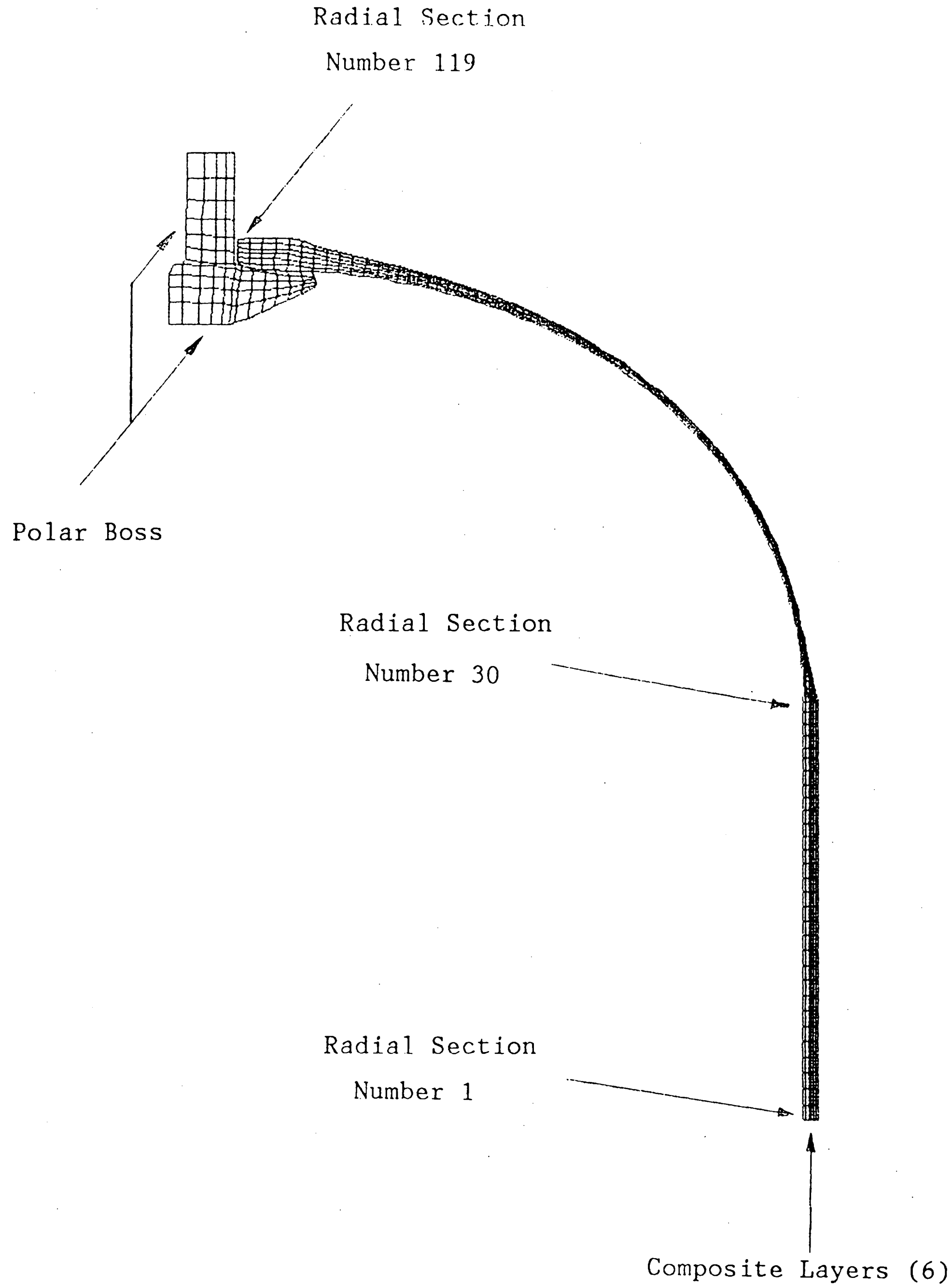

Figure 12. TASS preprocessor output showing composite layers and polar boss.

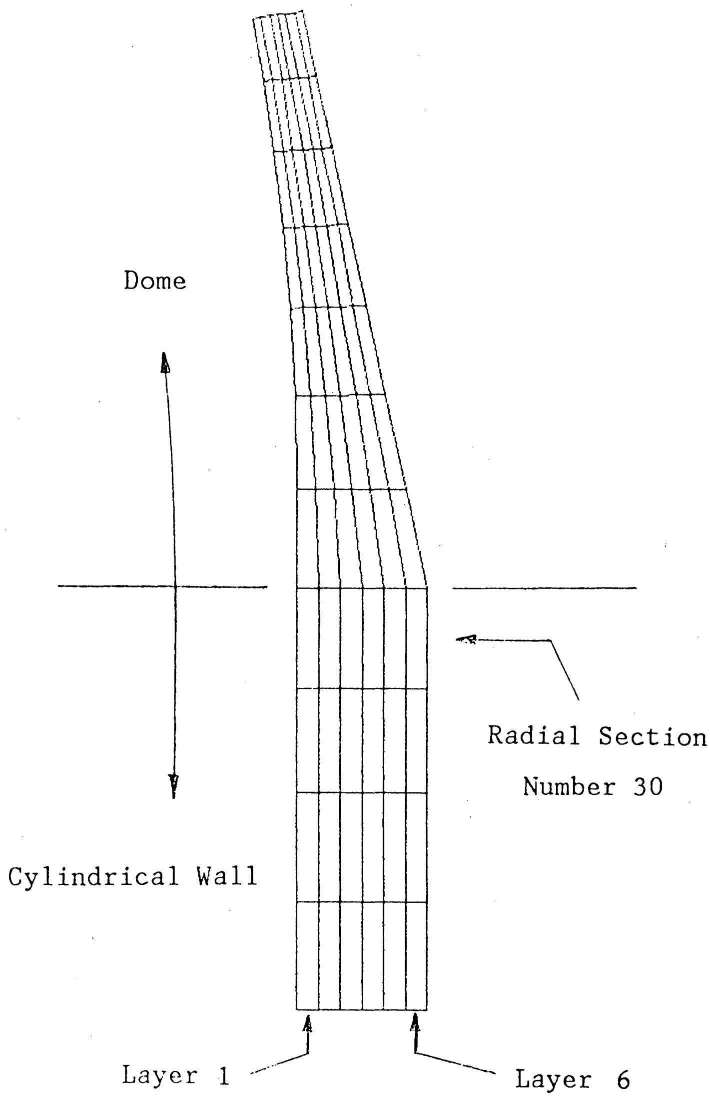

Figure 13. Transition between cylindrical wall and dome regions.

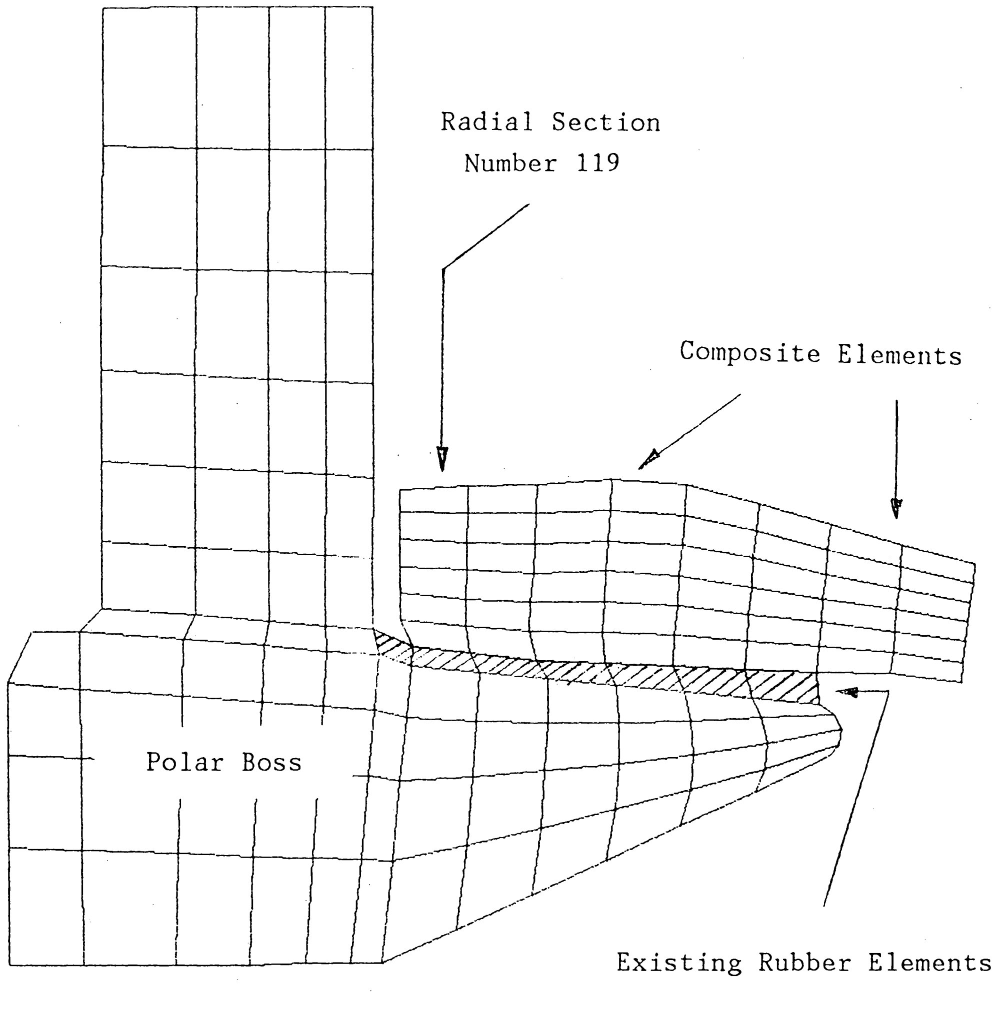

Figure 14. Transition between composite layers and polar boss region: The existing rubber interface elements are shaded for clarity.

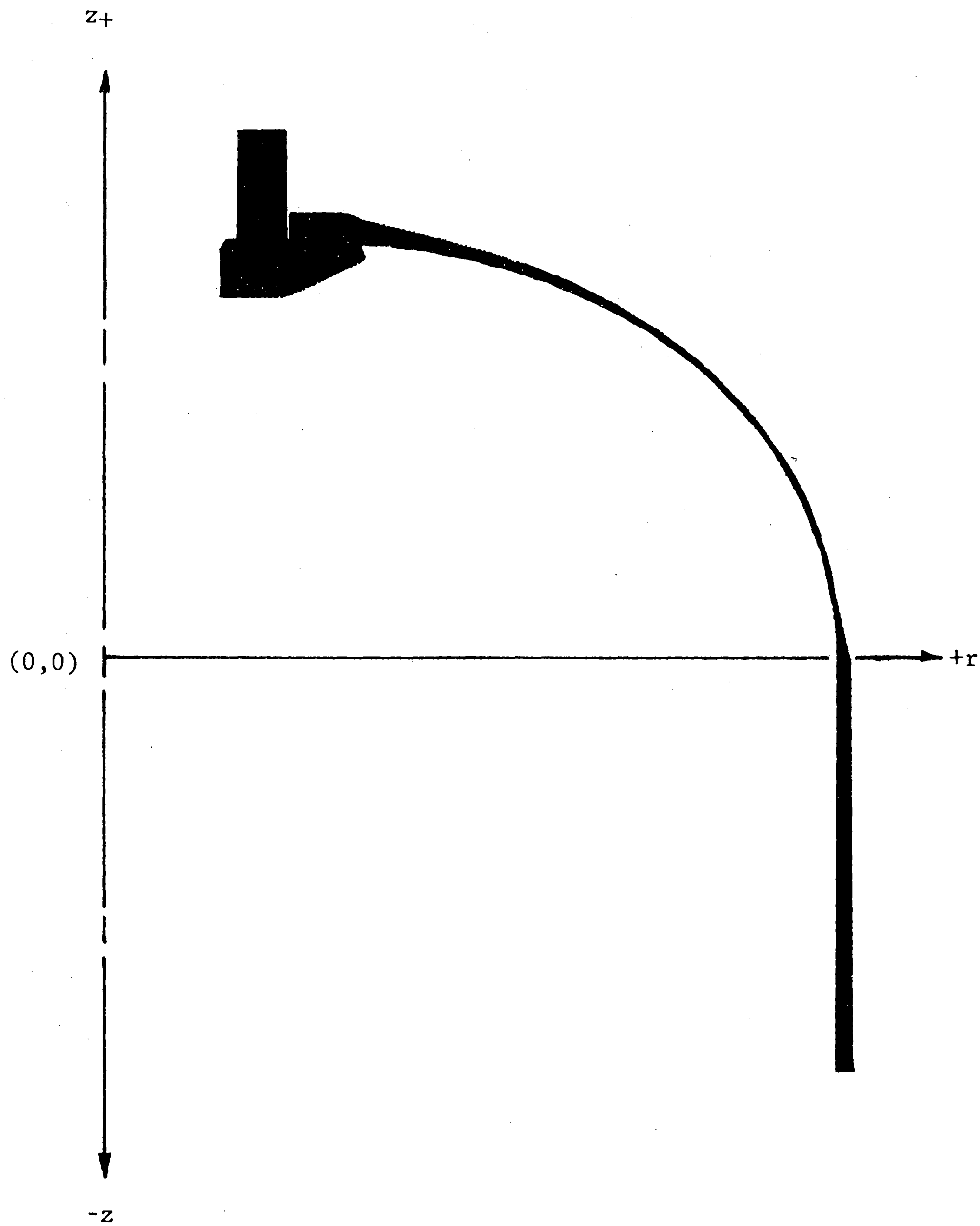

Figure 15. Cylindrical coordinate system used by TASS preprocessor

the radial coordinate while the plane defined by the beginning of the dome region is the zero reference for the axial coordinate.

The node and element numbering system used by TASS is based on the assignment of i,j indices to each element. The nodes are also assigned i,j indices that are determined relative to the element. This numbering system must be converted to the conventional counterclockwise system used by the WACSAFE finite-element program. This conversion is performed in two steps. First, a TASS utility program converts the geometry data to a clockwise sequential system and then the WACFORM preprocessor permutes the element definitions to a counterclockwise system. Figure 16 illustrates these numbering conventions.

5.3 TASS MATERIAL

The material data provided by TASS is divided into two parts; (1) a material number for each element in the geometry file and (2) a material file associating each material number with a wrap angle and a set of material properties.

The material number is found on each element data line along with the connectivity array and the angle SETA. Unfortunately, the file assigning material numbers to wrap angles and property sets is incomplete. Some material number references are not included in the material file and need to be generated.

Another difficulty encountered is that all the elements in the cylindrical region are assigned the same material number with no distinction being made between hoop and helically wound layers. The one number as-

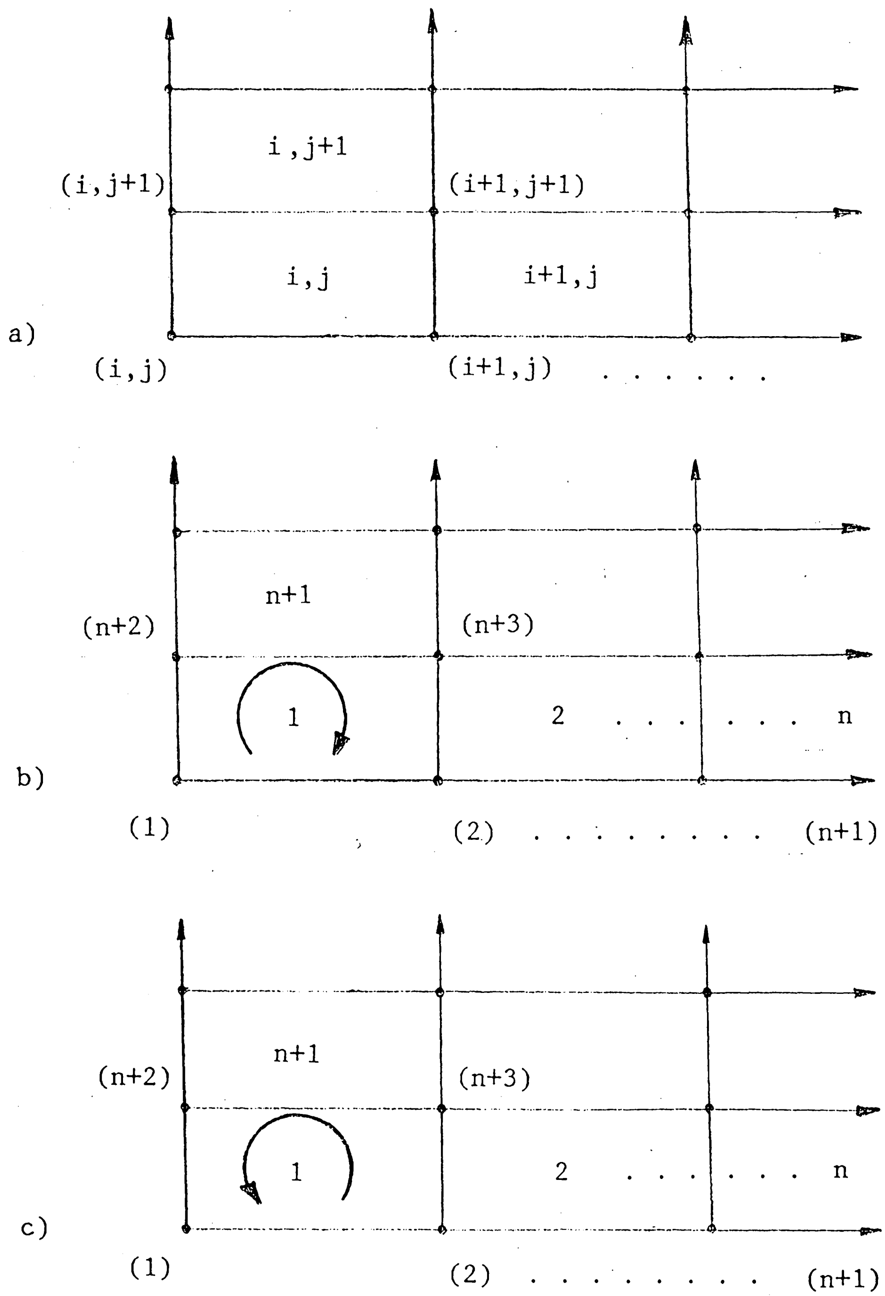

Figure 16. Node and element numbering conventions: (a) TASS i,j system. (b) clockwise sequential system. (c) WACSAFE counterclockwise sequential system.

signed refers to a set of averaged material properties. These averaged properties can not be used as input and therefore the cylinder material data must be reconstructed.

The wrap angle in the material file (designated ALPHA) is defined as the angle that a band of fibers form with a line of longitude on the bottle. The supplement of ALPHA is the fiber angle BETA used in WACSAFE. The angles ALPHA and BETA are shown in Fig. 17.

Lastly, the TASS material file does not contain any thermal expansion coefficients for the polar boss or the composite layers. These too must be generated.

5.4 WACFORM DATA PREPROCESSOR

The problems discussed in the previous sections were eliminated by developing the WACFORM preprocessor. The capabilities of this program are listed below:

1. Read and plot the TASS geometry file
2. Read TASS material file
3. Generate additional material numbers and sets
4. Generate mandrel and rubber elements
5. Plot the new model geometry sorted by:
    - Element number
    - Material set
    - IOFFON number
6. Write complete WACSAFE input file

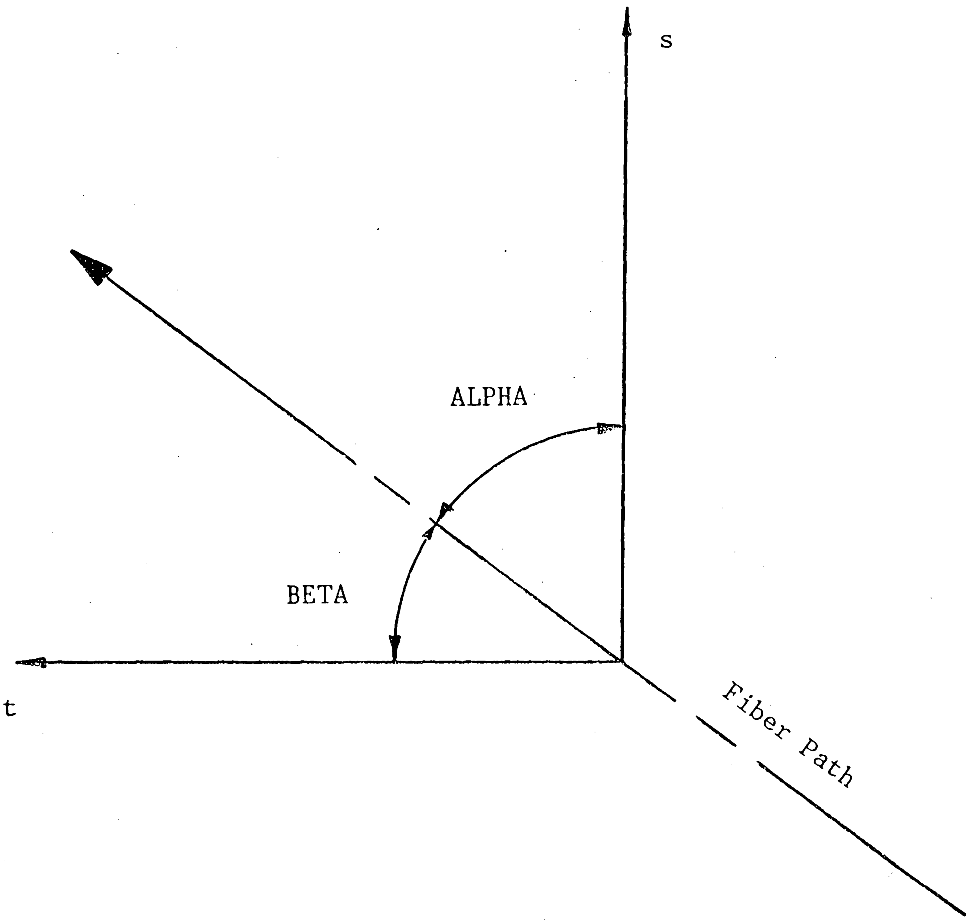

Figure 17. Relationship between angles ALPHA and BETA.

The geometry plots in this work are generated from the preprocessor.

All the preprocessor functions are directed from a control file. The control file describes the TASS geometry and material files. The control file also directs the generation of additional data. Details and examples of the data format of this file are found in the WACFORM users guide [12].

For simplicity the preprocessor works with a mesh that is viewed as if all the SETA angles are equal to 90°. Figure 18 illustrates this perspective. In this perspective, the TASS geometry can be described in term of rectangular node and element sections. A single node section is any rectangular region of nodes that span the model thickness. A single element section is any rectangular region of elements that span the model thickness with the added restriction that there is no horizontal variation of material numbers. Figures 19 and 20 show the node and element sections in an exploded view that are used for the 18 in. (457mm) bottle problem.

The generation of mandrel and rubber element nodes is controlled by building a node section data table and specifying the thickness of each additional layer (Table 2). The generation of the mandrel and rubber elements is controlled by building an element section data table (Table 3). The information contained in these tables is explained in greater detail in the following paragraphs.

The node section data table contains an entry line for every node section in the model. Every entry line contains the section number, the section height in nodes, the section width in nodes, and the number of additional nodes to be generated. Nodes are generated by computing a direction vector and using a simple slope-distance equation to generate

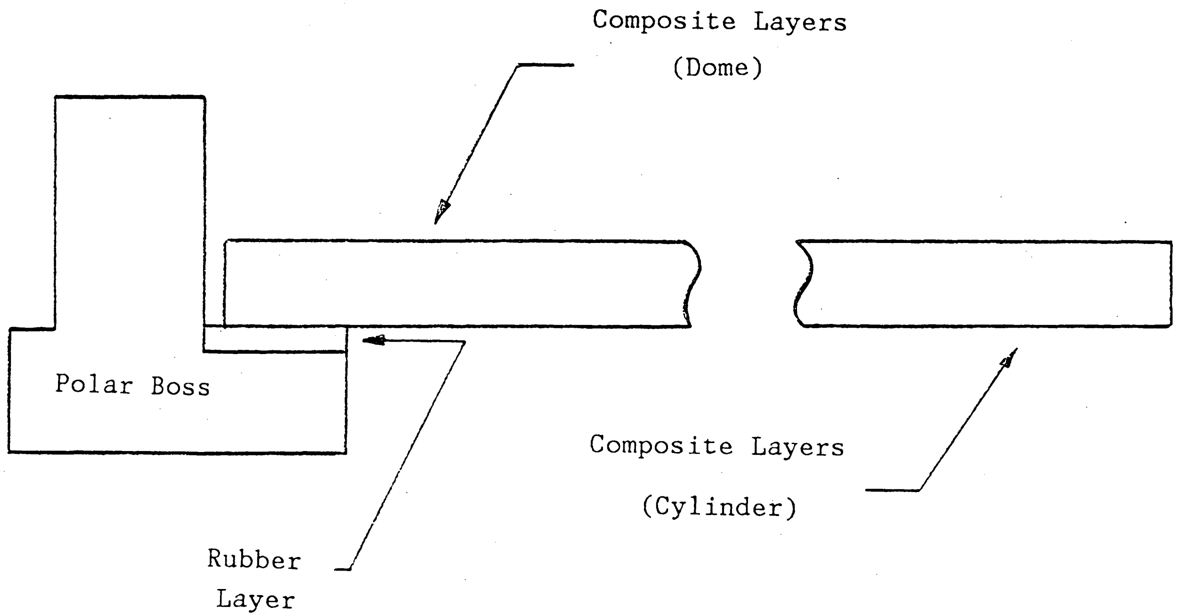

Figure 18. Model viewed with all orientation angles equal to 90°.

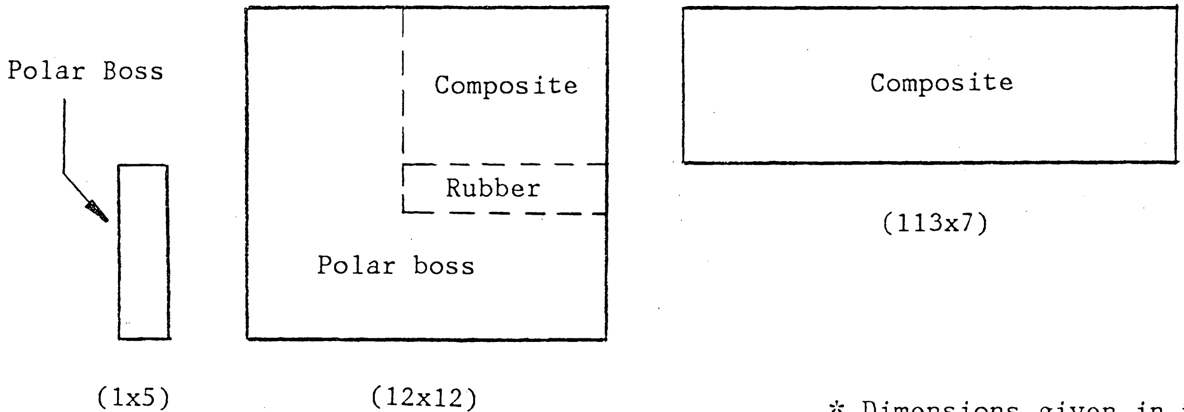

* Dimensions given in nodes

** (width x height)

Figure 19. Exploded view of nodal sections.

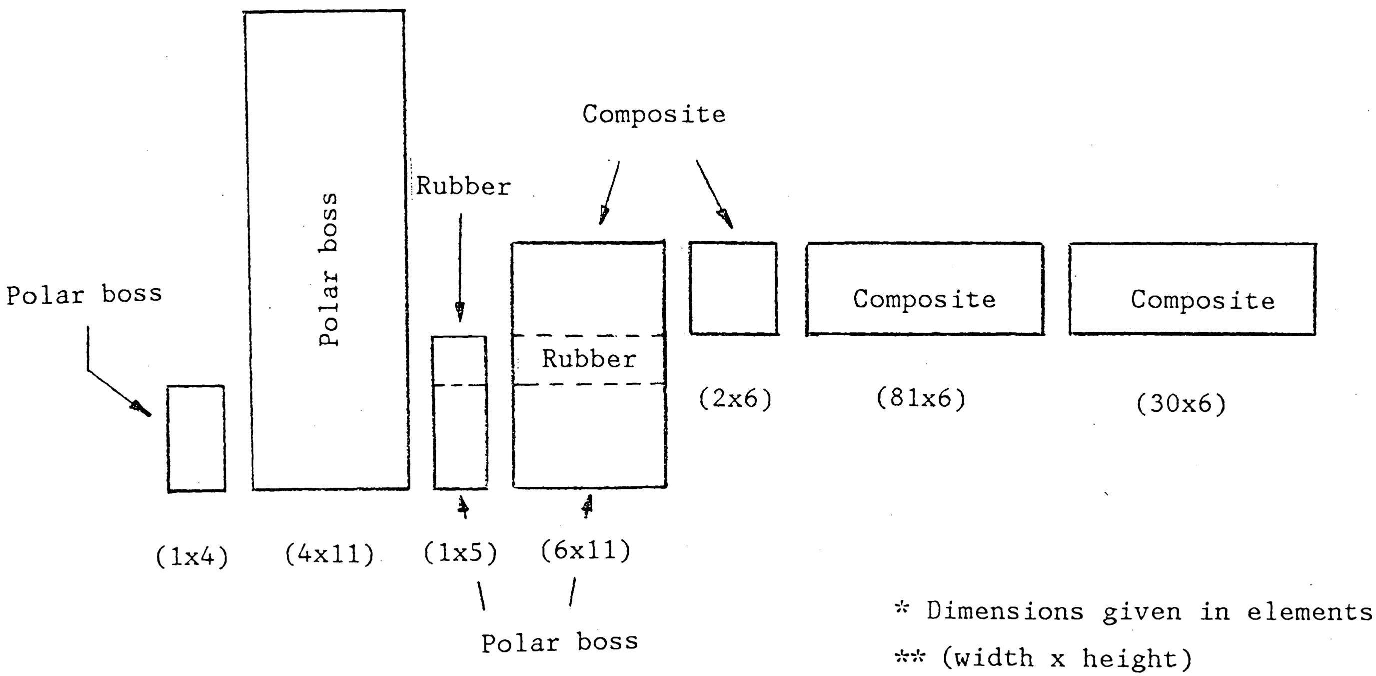

Figure 20. Exploded view of element sections.

Table 2. Nodal section data and generation thicknesses.

SECTION NUMBER	SECTION HEIGHT (NODES)	SECTION WIDTH (NODES)	NUMBER OF ADDITIONAL LAYERS
1	7	113	4
2	12	12	3
3	5	1	3

SECTION NUMBER	ADDITIONAL LAYER THICKNESS (IN.)			
	LAYER 1	LAYER 2	LAYER 3	LAYER 4
1	0.9	0.5	0.15	0.060
2	0.9	0.5	0.060	*
3	0.9	0.5	0.060	*

Table 3. Element section and material assignment data.

SECTION			EXISTING			ADDED	
NO.	HEIGHT	WIDTH	MANDREL	RUBBER	COMPOSITE	MANDREL	RUBBER
	(NUMBER OF ELEMENTS)						
1	6	30	0	0	6	3	1
2	6	81	0	0	6	3	1
3	6	2	0	0	6	2	2
4	11	6	4	1	6	2	1
5	5	1	4	1	0	2	1
6	11	4	11	0	0	2	1
7	4	1	4	0	0	2	1

the new nodal coordinates. The first and fourth existing nodes in a node column are used to define the generation direction. The fourth node is used instead of the second or third because the greater spacing between nodes reduces the sensitivity of the direction calculation to small errors in the existing nodal coordinates.

The element section table also contains an entry for every element section. Each entry line contains the section number, the section height in elements, the section width in elements, the number of existing mandrel elements, the number of existing rubber elements, and the number of existing composite elements or layers (one layer is one element thick). In addition, each entry line contains the number of additional mandrel and rubber elements to be generated.

After the above information is read, the new total number of nodes and elements is computed. The node and element data arrays are then expanded to accommodate the generated data and the generation proceeds.

The cylindrical section data is then reconstructed by first defining all the layers as hoop layers and then modifying those layers that should be helically wound. The number of layers that will be made into helicals is read from the control file along with the layer numbers, the wrap angle ALPHA and the material set number. In this case, the data from the first element column in the dome portion was used for all the cylindrical element columns.

The initial stress in the composite layers is then read from the control file and the value inserted into the element data array. Unfortunately, the element numbering proceeds radially outward along each element column, which means that the elements making up a layer are not found sequentially in the element data array. Therefore, when inserting the tension data into the element array, a constant offset must be computed for each element section which takes into account the number of existing and generated mandrel, rubber and composite layers.

Two options exist for assigning boundary conditions to the model. The inside surface of the mandrel elements can be rigidly fixed in both r and z directions or the surface can remain free. In both cases, the boundary defined by the equatorial plane is fixed in the z direction and free in the r direction. The boundary condition option is specified by simply inputting a 1 for fixed or a 0 for free on the boundary condition line in the control file.

Lastly, the preprocessor writes a complete input file for the finite-element program. The default values for other program parameters are discussed in the program users guide [12].

6 RESULTS AND DISCUSSION

The finite-element program WACSAFE was used to determine the residual stress state in a filament wound graphite/epoxy bottle after the fabrication process. A description of the actual bottle and the finite-element model are first presented, followed by the program results. The program results are discussed as they are presented.

6.1 BOTTLE DESCRIPTION

The bottle considered is wound on a cast sand/PVA mandrel which is covered with a 0.060 in. (1.52 mm) layer of rubber insulation. The rubber layer acts as an insulator when the bottle is in service. The mandrel and rubber together have an outside radius of 9.0 in. (228 mm) which corresponds to the inside radius of the finished structure. The graphite/epoxy windings form a wall thickness of 0.060 in. (1.52 mm) in the dome and 0.171 in. (4.35 mm) in the cylindrical region. The wrap angle BETA is 77° on the cylinder and in the first element section in the dome. Moving up the dome toward the vertical axis, the wrap angle decreases to a minimum value of 0° at the last element section where the polar boss begins (Fig 12).

The spool tension is specified at 5 to 7 lbs (22-31 N) for a fiber cross section of $3.85 \times 10^{-4} in^2$ ($9.78 \times 10^{-3} mm^2$). The spool tension is the tension in the fibers as they leave the feed spool. Using the median value of 6 lbs (27 N), the spool stress in the fibers is calculated to be 15.6 kpsi (107.6 MPa). The actual stress value used in the finite-element analysis is 50 percent of the spool value or 7.9 kpsi (53.8 MPa). The reduction accounts for the loss of winding tension immediately following application to the model. This behavior was discussed by Knight and Leavesley [1] and an empirical curve presented.

6.2 GENERATING THE COMPLETE MODEL

The mesh provided by the TASS preprocessor consists of the composite layers, the polar boss and a small fraction of the rubber insulation elements (Fig. 14). The details of this mesh were given in the previous chapter.

A new mesh was generated to include mandrel elements and additional rubber elements. The new mesh consists of 1431 nodes and 1285 elements, an increase of approximately 35 percent. Figure 21 shows the full finite-element mesh for the bottle.

The first node and element are found at the lower left corner of the cylindrical wall. The node and element numbering proceeds radially outward starting at the equatorial plane and ending at the inside surface of the polar boss. Figures 22 and 23 are enlarged portions of the full mesh showing important features and detail. First, note the triangular gap in the mesh at the outer rim of the polar boss seat in Fig. 23. This gap was intentionally generated to eliminate problems that would arise during both node and element generation in this area. This problem results from the large concentration of nodes at the point formed by the outer rim of the polar boss seat. The effect that this gap has on the

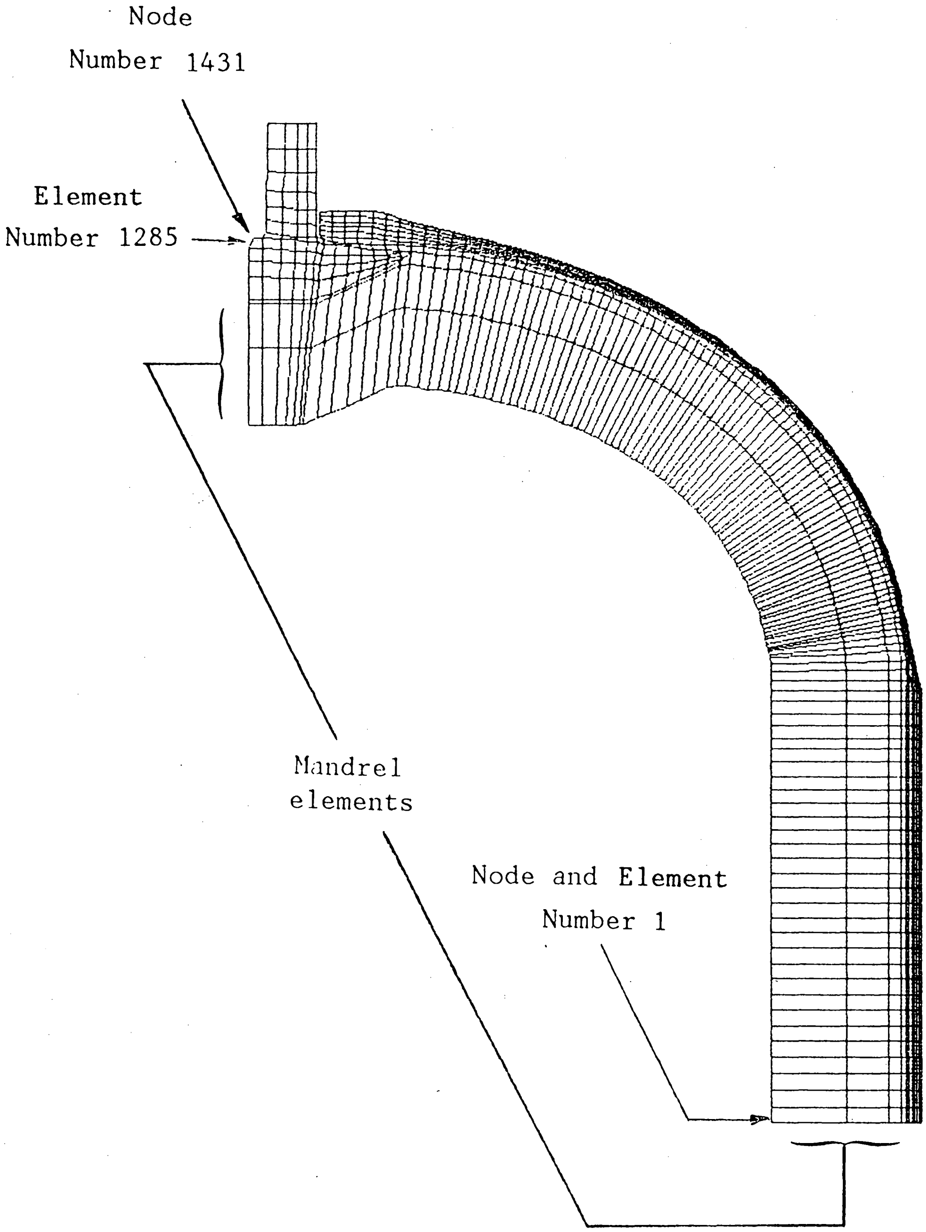

Figure 21. Full finite-element mesh of 18 in. (457 mm) bottle.

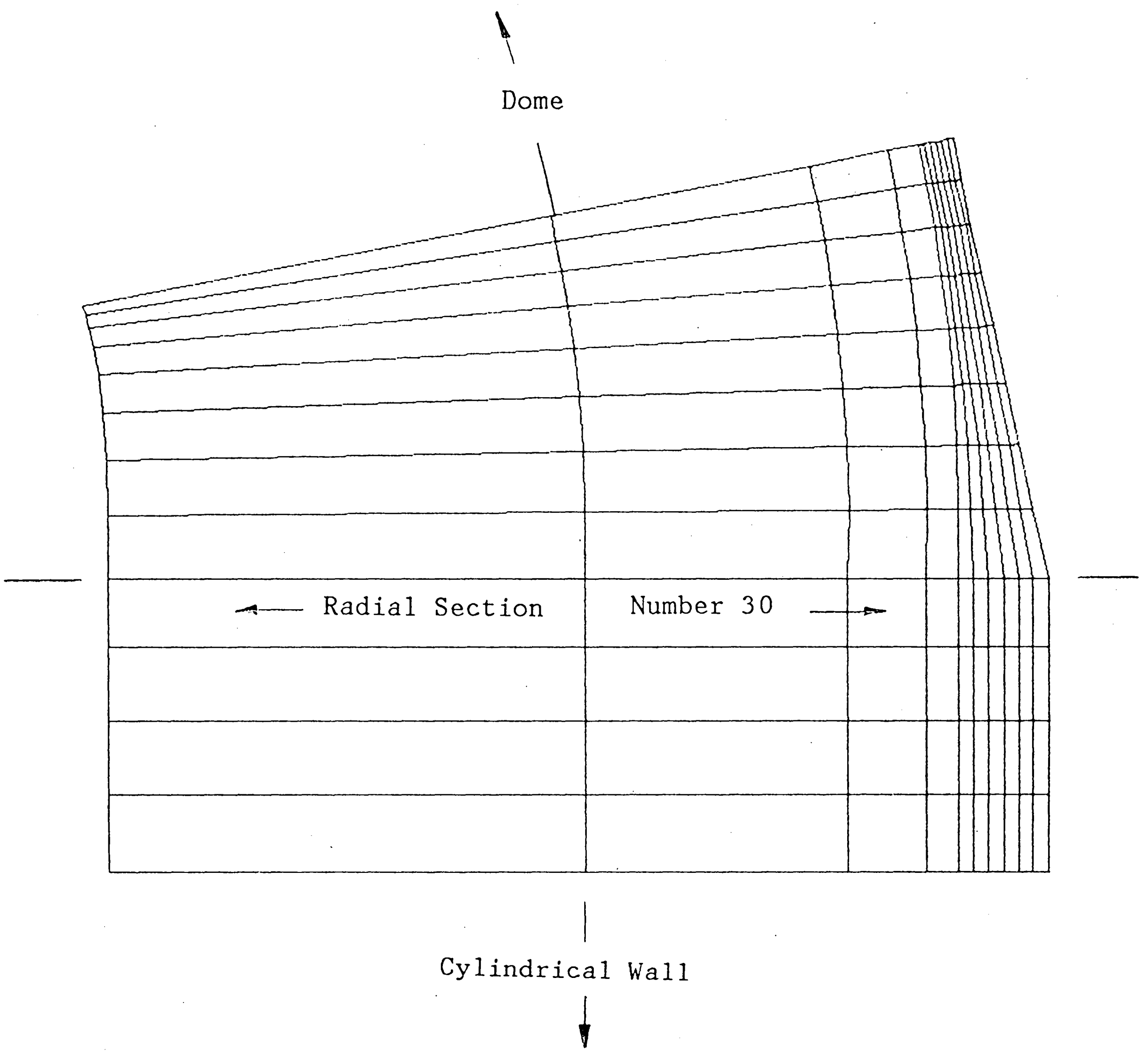

Figure 22. Transition from cylindrical to dome region for full mesh.

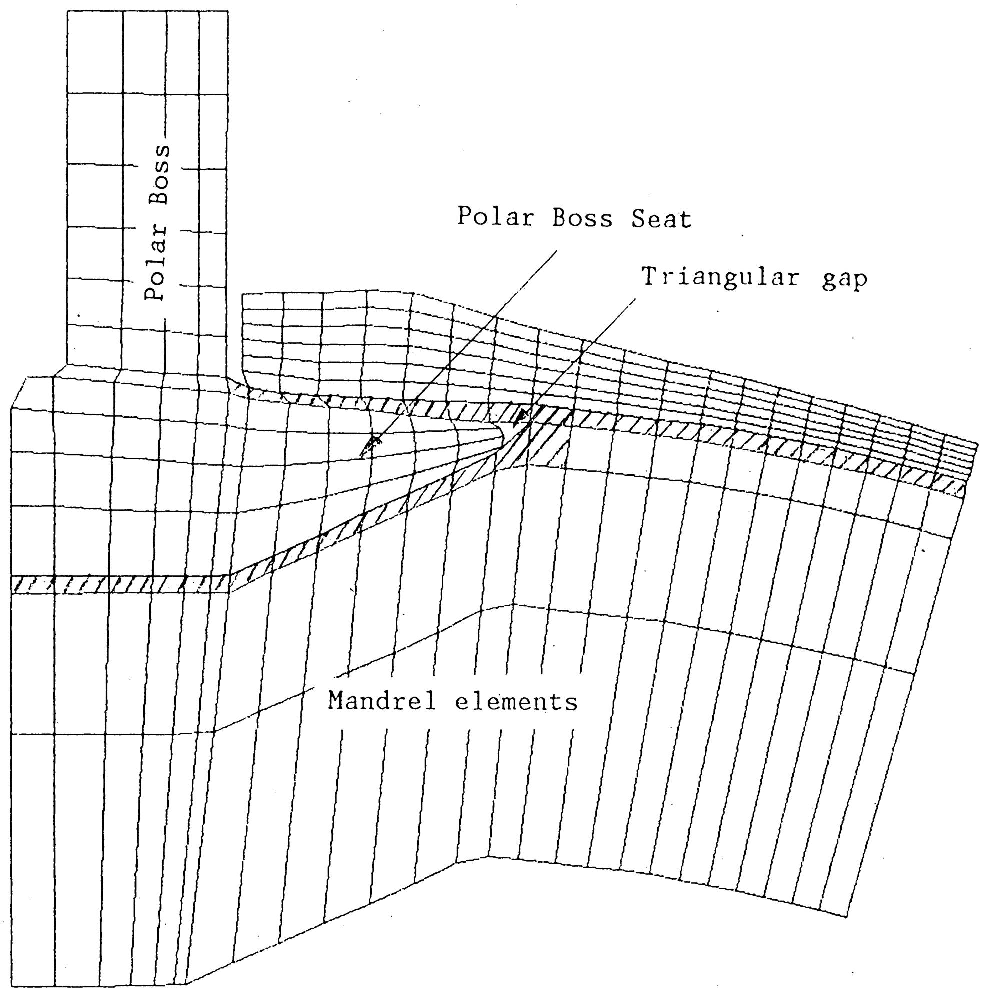

Figure 23. Transition between composite layers and polar boss region: Both original and generated rubber interface elements are shaded for clarity.

stress results is negligible because the area where it occurs is very small. The possibility existed that the gap might cause the global stiffness matrix to become non-positive definite, however, such was not the case. Also note that the polar boss and the last section of composite elements are not attached to one another. A consequence of this is that the last composite element section represents a free edge where the stresses will be different than adjacent composite elements. Lastly, note that the composite thickness becomes greater directly over the polar boss seat. The increased thickness is due to the fact that all the helical layers pass through this area and tend to pile up on each other.

The generated mandrel elements are easily identified by comparing Fig. 21 with Fig. 12. The existing and generated rubber elements are shown isolated in Fig. 24. This plot was produced by using the plot material option of the preprocessor.

The helical and hoop data in the cylindrical wall was reconstructed and merged with the remaining geometry and material data. As can be seen in Fig. 25, which shows the hoop layers removed and enlarged slightly, there are two hoop layers sandwiched between four helical layers. The hoop layers extend two element sections into the dome. Two hoop layers were generated because the difference in average wall thickness in the cylinder and dome is approximately the thickness of two element layers in the cylinder. This results in a total hoop layer thickness of 0.057 in. (1.45 mm) while the total helical layer thickness is 0.114 in. (2.9 mm). Placing the hoop layers between the helicals was decided upon without any concrete specifications. However, the choice seems reasonable considering the fact that while the hoop layers are probably not all

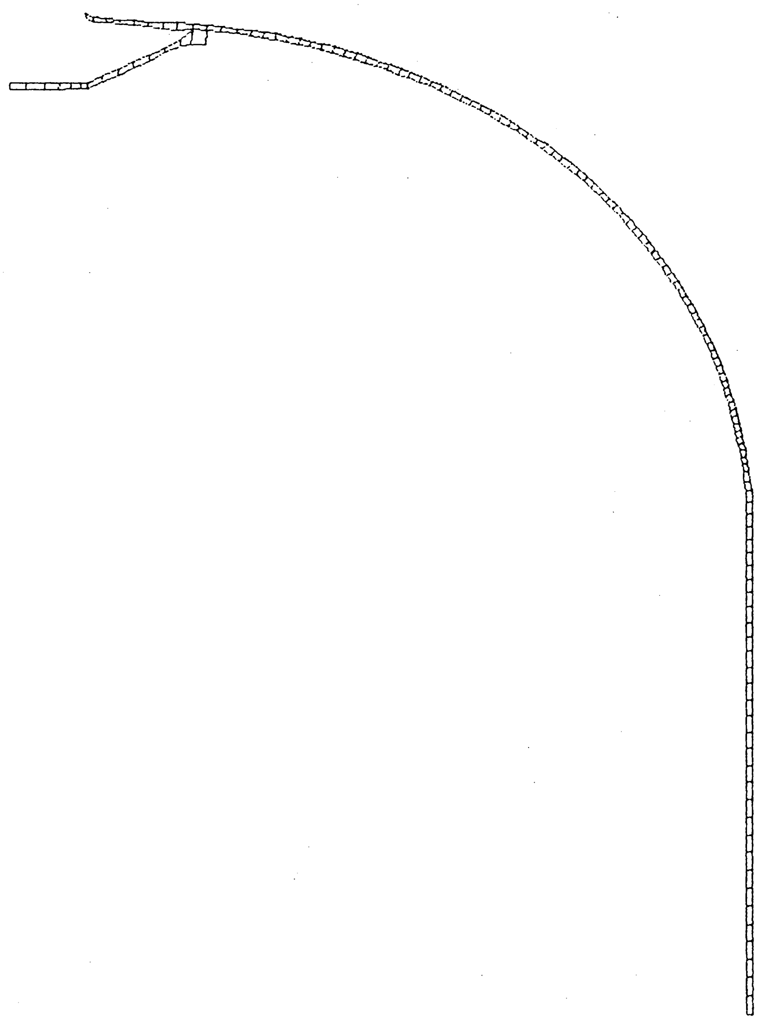

Figure 24. Rubber interface elements for full model.

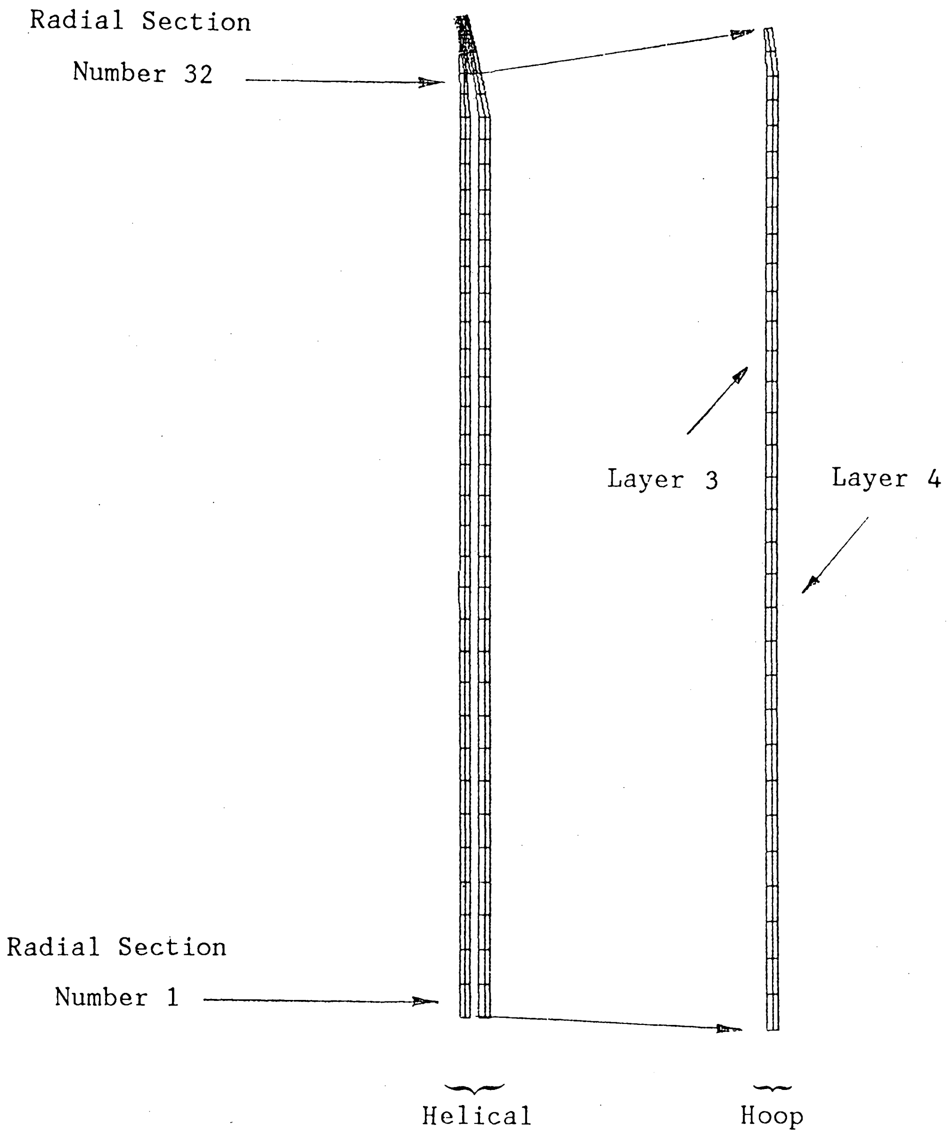

Figure 25. Cylindrical wall showing hoop and helical element layers.

lumped into one thick layer, the majority of them would be found somewhere between helical layers.

Several different placements of the hoop layers, including total elimination of all the hoop layers, were examined. However, only the placement mentioned was considered here.

The plot material option mentioned previously proved to be a very useful diagnostic tool during the mesh generation. For example, the rubber element plot (Fig. 24) provides visual verification that both the generation and assignment of material numbers for the rubber layer were successful. Also, Fig. 25 verifies the reconstruction of hoop and helical data in the cylindrical wall. Similar plots for the composite layers, polar boss and mandrel elements are possible.

The material properties used in this analysis are summarized in Table 4. The radial stiffness for the uncured material is reduced to better approximate the wet fiber/resin system [1]. The thermal coefficients are taken from a T300/5208 graphite/epoxy system.

6.3 FINITE-ELEMENT PROGRAM RESULTS

Two different mandrel models were analyzed using the WACSAFE finite-element program. First, the composite layers were wound onto a rigid steel mandrel with no additional rubber elements. This model was chosen as the first test case because the behavior of the composite layers and steel mandrel during both the winding and curing stages is predictable. The second model utilizes the same geometry but with the softer sand/rubber mandrel. In this model the behavior of the mandrel and com-

Table 4. Material properties of the graphite/epoxy model.

GRAPHITE FIBERS (uncured)

E1	=	18.7×10^{6} psi	(129 GPa)
E2	=	11.2×10^{5} psi	(7.72 GPa)
E3	=	5.6×10^{5} psi	(3.86 GPa)
ν_{23}	=	0.3000	
ν_{31}	=	0.0161	
ν_{21}	=	0.0085	
G12	=	7.3×10^{5} psi	(5.03 GPa)
$\alpha 1$	=	-4.30×10^{-7} /°F	(-7.74×10^{-7} /°C)
$\alpha 2$	=	1.36×10^{-5} /°F	(2.45×10^{-7} /°C)
$\alpha 3$	=	1.36×10^{-5} /°F	(2.45×10^{-7} /°C)

GRAPHITE FIBERS (cured)

SAME AS UNCURED EXCEPT FOR THE RADIAL MODULUS

E3	=	11.2×10^{5} psi	(7.72 GPa)

POLAR BOSS (steel)

E1	=	29.0×10^{6} psi	(200 GPa)
ν	=	0.3000	
α	=	6.50×10^{-6} /°F	(11.7×10^{-6} /°C)

SAND/PVA (mandrel)

E1	=	8.75×10^{2} psi	(6.03 MPa)
ν	=	0.3000	
α	=	-3.10×10^{-6} /°F	

RUBBER (mandrel)

E1	=	4.50×10^{2} psi	(3.10 MPa)
ν	=	0.4900	
α	=	9.00×10^{-5} /°F	(16.2×10^{-5} /°C)

posite layers during winding is also predictable, however, during cure the combination of thermal expansion coefficients for the mandrel, rubber and composite layers makes a prediction of the model behavior impossible.

The stress distribution in the composite layers was determined at; (1) the end of the winding stage, (2) the end of the heating cycle and (3) the end of the cooling cycle. Polymerization was assumed to occur after the heating stage.

6.3.1 STEEL MANDREL

The addition of composite elements to the finite-element model to simulate winding was performed in six steps, one for each layer of composite elements. First, the mandrel, polar boss and inner most layer of composite elements was turned on. The effective model at this point is shown in Fig. 26 (effective in that only these elements make significant contributions to the global stiffness matrix). The cylindrical wall section is not show in Fig. 26 for scaling purposes. The model is solved and the next layer added to the model until all six composite layers have been added.

After the sixth load step the residual stress in all the elements is output. Even with the output suppression option, the output listing is very long (over 6000 lines). Therefore, the data for the composite layers was extracted and plotted as a function of the element section number. Fig. 27 shows the fiber direction stress in each composite layer after the final winding step.

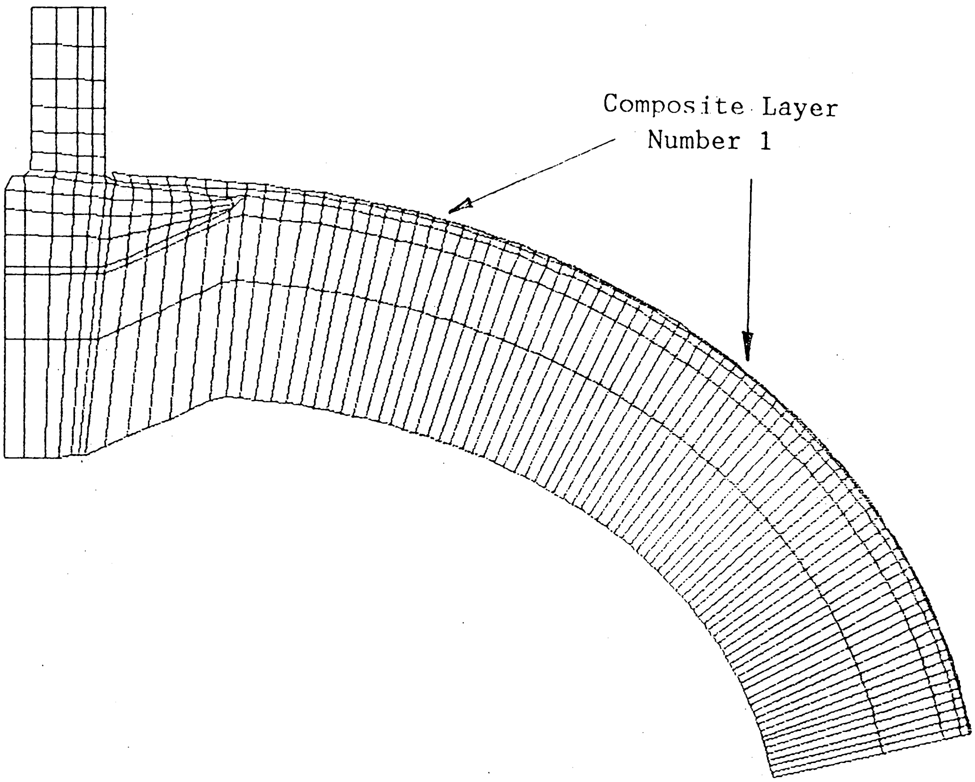

Figure 26. Effective finite-element model for first winding load step.

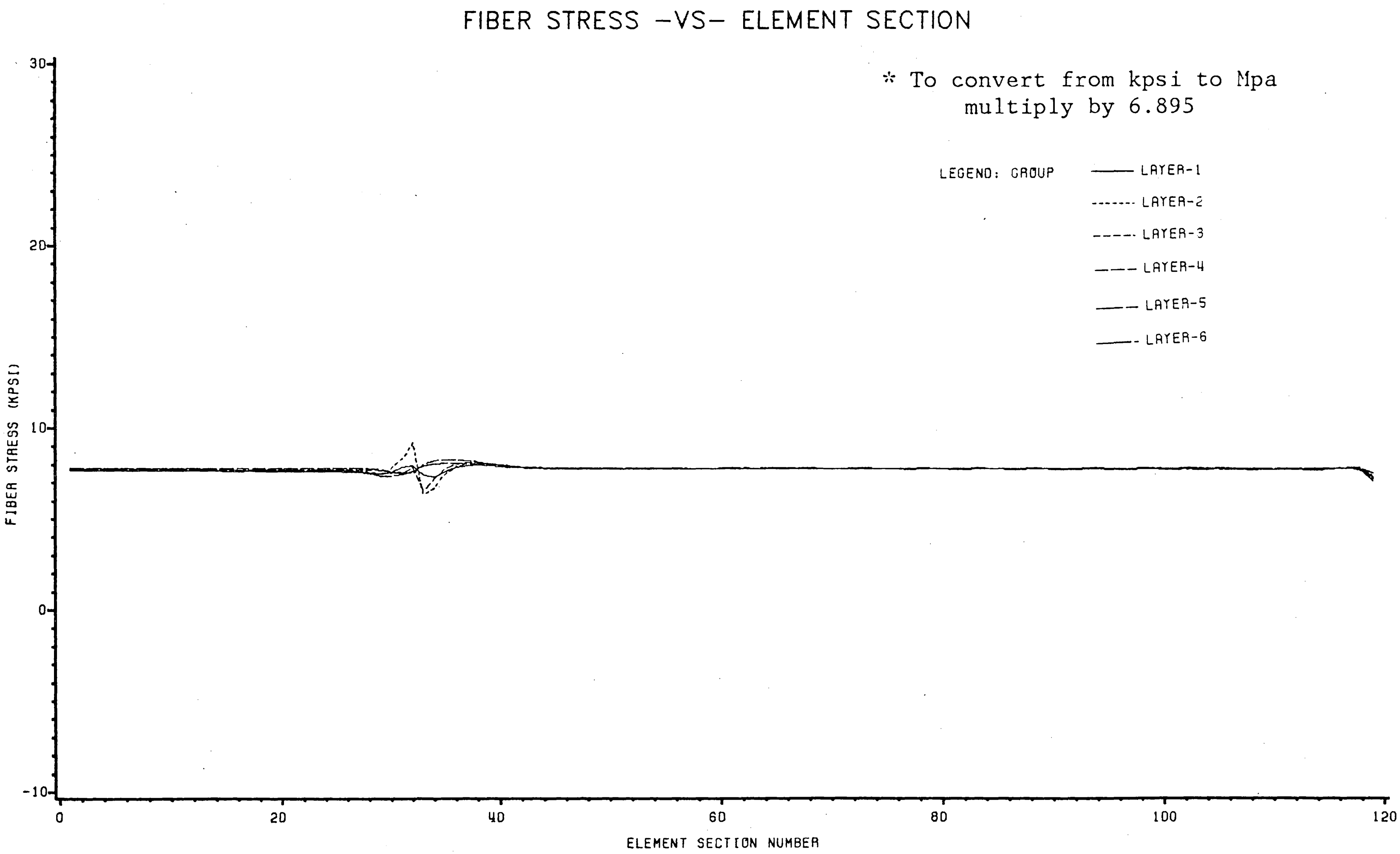

Figure 27. Layer stress curves for steel mandrel after winding.

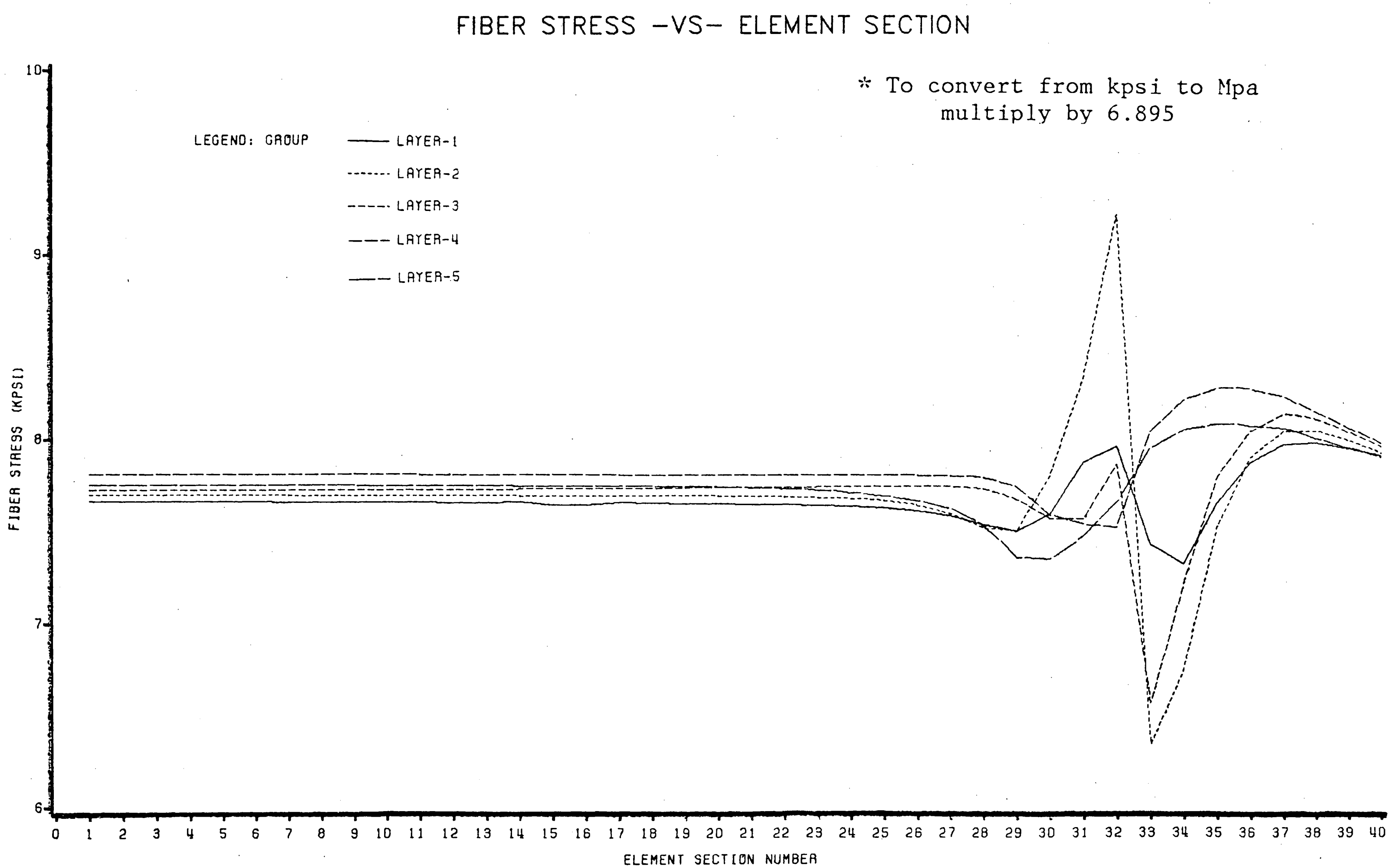

Figure 28. Enlarged view of first forty element section after winding.

The coherence of the layer stress curves show very little initial winding tension loss. This was expected because the steel mandrel is very rigid and does not deflect appreciably under the influence of the radial pressure due to winding. The discontinuity between the last hoop elements (radial section 32, layers 3 and 4) causes the disruption around section 32. Fig. 28 is an enlarged view of the first forty sections. This figure shows that there is a slight loss of initial tension in the helical layers and the inner hoop layer. However, it is interesting to note that the outer hoop layer experiences an increase in initial stress. This is attributed to the discontinuity of fiber angles between the hoop and helical layers and the overall geometry of the bottle.

The model was then subjected to a uniform increase in temperature of 150 ^{o}F (65.5 ^{o}C) from a reference temperature of 70 ^{o}F (21 ^{o}C) to simulate the heating cycle. The material during this cycle is still uncured. Figure 29 shows the layer stress curves at the conclusion of the heating cycle.

The hoop layers are clearly visible in this figure because they tend to support a greater percentage of the stress load due to the thermal expansion of the steel mandrel (27 kpsi (190 MPa) compared to 16.6 kpsi (114 MPa) for the helical layers). Also, the free edge at section 119 shows higher stresses (25 kpsi (170 MPa) compared to 11 kpsi (76 MPa)) then the surrounding elements.

Of prime importance is the fact that for a mandrel that expands upon heating the stress level in the composite layers increase. Therefore, even if some layers had experienced a total loss of initial winding tension, the expanding mandrel would drive them back into tension before the

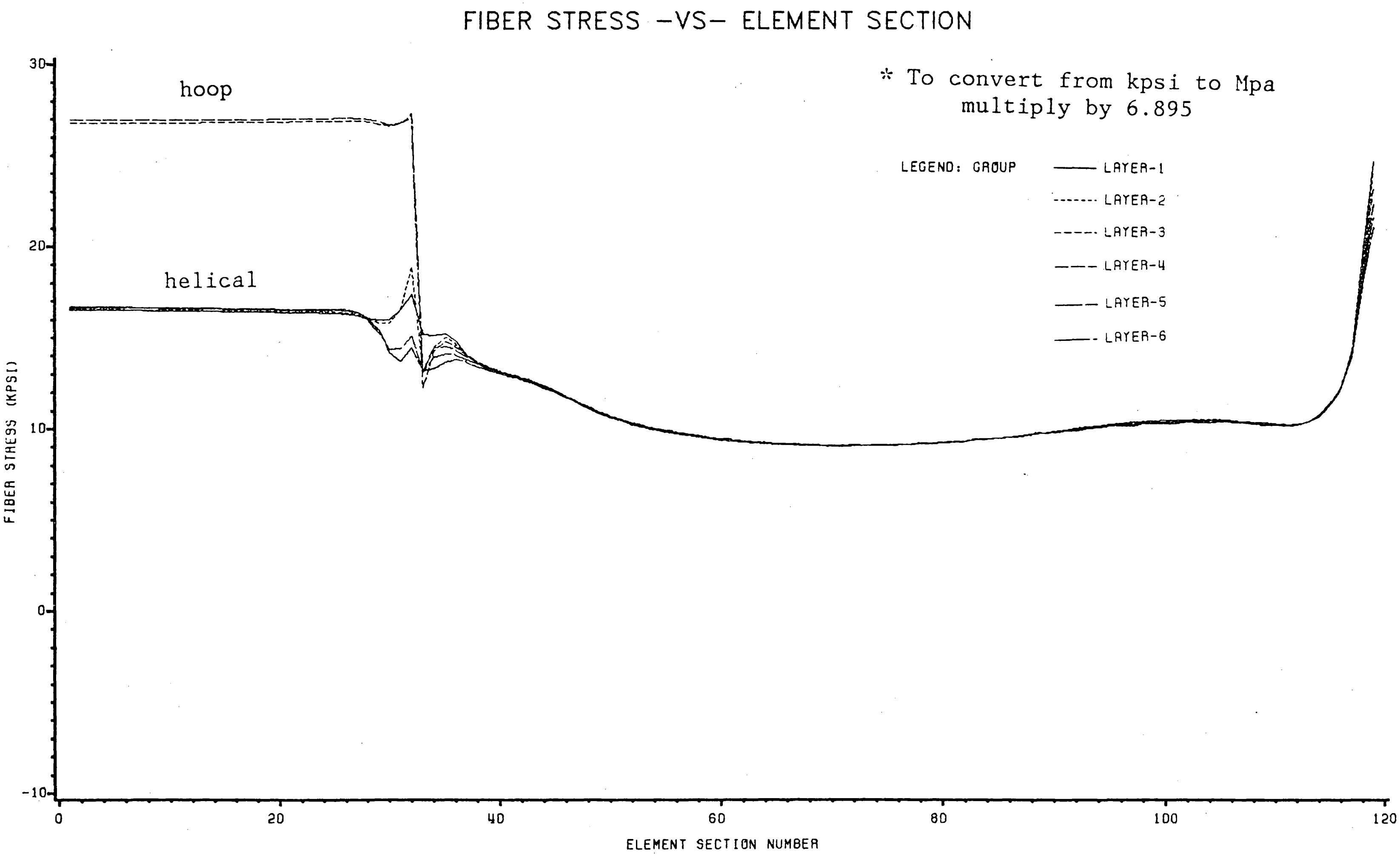

Figure 29. Layer stress curves for steel mandrel after heating.

material cured. It has already been reported [1] that a filament wound structure should have residual tension in all the fibers before curing if accurate strength predictions are to be made. Although the steel mandrel in this case is very thick, it is reasonable to assume that similar behavior will occur for thinner (to a limit) steel mandrels.

Lastly, the model was subjected to a uniform drop in temperature of 150 ^{o}F (65.5 ^{o}C). Figure 30 shows the layer curves after cooling. The reason that Fig. 30 is not a duplicate of Fig. 27 is that the material has cured and cured material properties and stress algorithms were used. In fact, Fig. 30 more closely resembles Fig. 29 with a uniform translation downward of 20 kpsi (140 MPa).

It should be noted that in the actual fabrication process, the contracting steel mandrel is not rigidly bonded to the rest of the structure and therefore the composite layers would not be pulled into compression to such a degree as is predicted in Fig. 30.

6.3.2 SAND/RUBBER MANDREL

The same three cases were run for the sand/rubber mandrel. The same mandrel geometry was used but different material numbers were assigned to the elements as was discussed in the first section of this chapter.

The residual stress state in the composite layers at the conclusion of the winding stage is shown in Fig. 31. These curves show that there is significant loss of initial winding tension in the composite layers. The entire first layer exhibits compressive fiber direction stress aver-

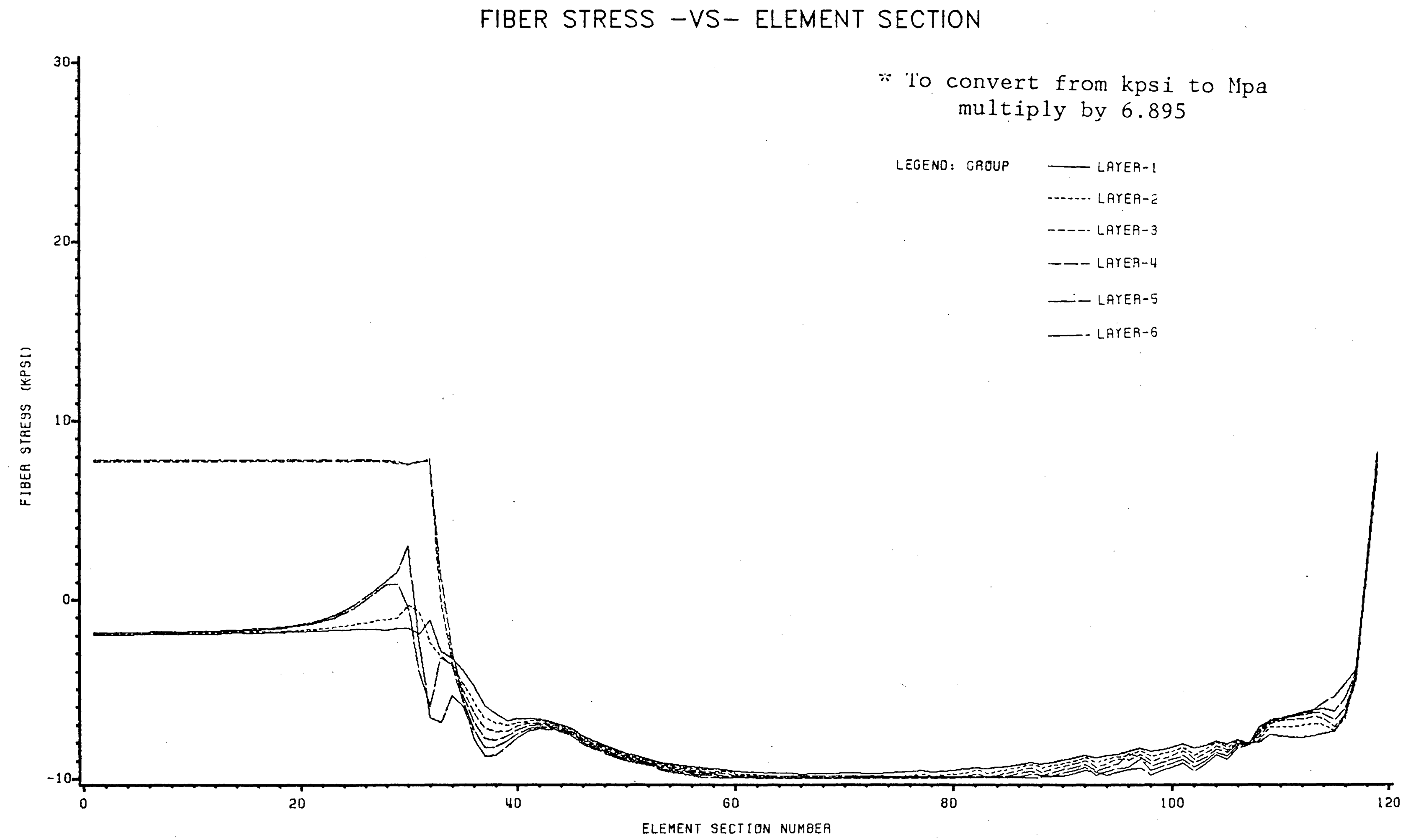

Figure 30. Layer stress curves for steel mandrel after cooling.

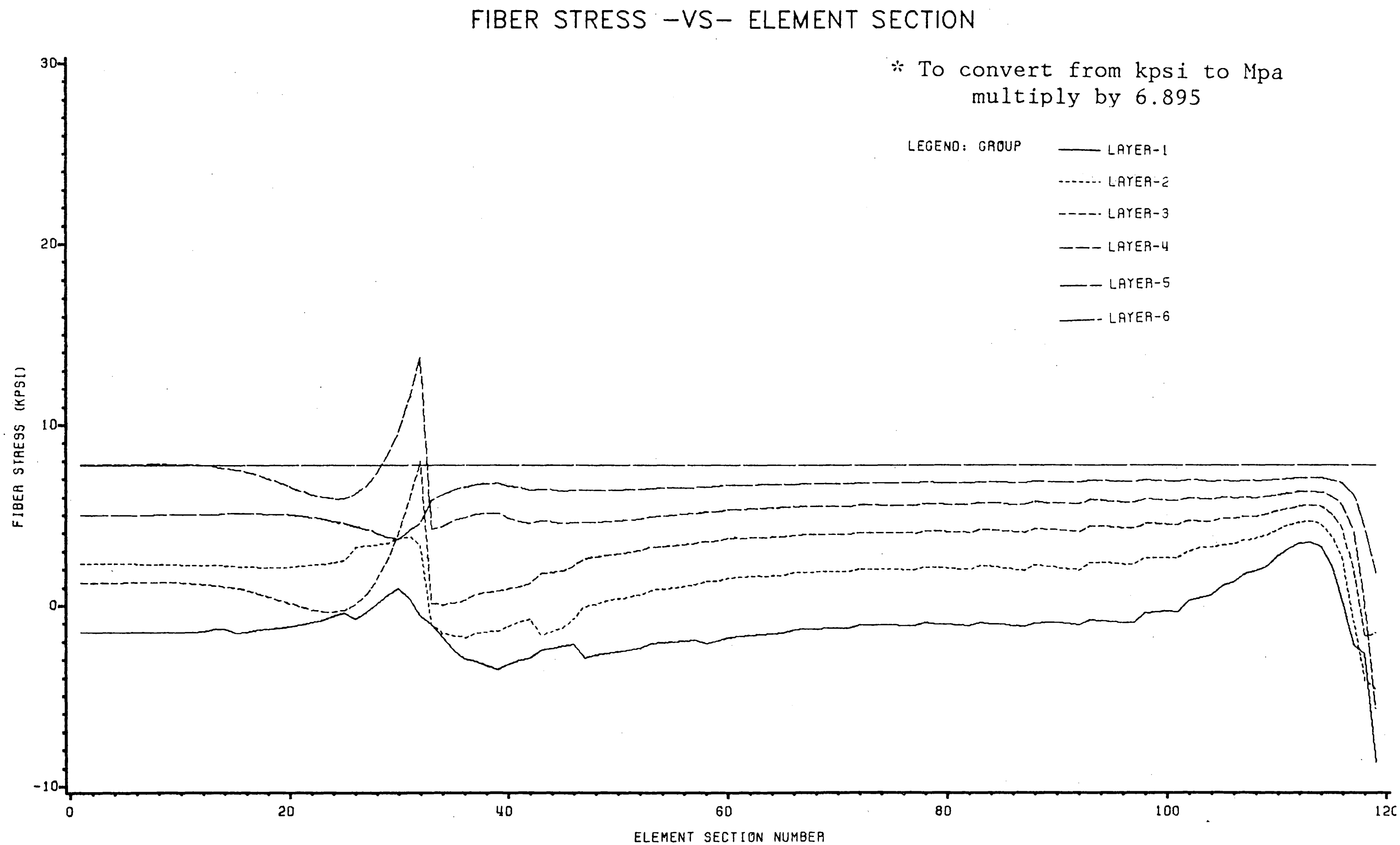

Figure 31. Layer stress curves for sand/rubber mandrel after winding.

aging about -1.0 kpsi (-6.9 MPa). The other layers have reduced (but still tensile) fiber direction stress present.

The pattern of tension loss in the dome region is well behaved with the inner layers losing more tension then those nearer the outer surface. The horizontal line for layer six is the residual spool tension which was input to the program. The slight oscillation of the stress curves in the dome region is attributed to the discrete values of the polar orientation angle (SETA) in this region.

More interesting to note is the behavior in the cylindrical wall region. The helical layers exhibit predictable tension loss patterns. However, the hoop layers both show a characteristic dip at section number 24 followed by a spike (14 kpsi (96 MPa)) at section number 32. Again this is caused by the discontinuity at the termination of the hoop section.

Also note that the outer hoop layer experiences an increase in residual tension, while the inner hoop layer loses more tension then the underlying helical layer. Similar behavior was exhibited in the steel mandrel case, but to a much lesser degree. This occurs because mandrel deflection will affect hoop layers more so then helical layers. This pattern looks very reasonable.

Next the model was subjected to the same rise in temperature as in the steel mandrel model. However, because of the negative thermal expansion coefficient of the sand and the large thermal coefficient of the rubber, the stress curves in Fig. 32 behave differently then for a steel mandrel.

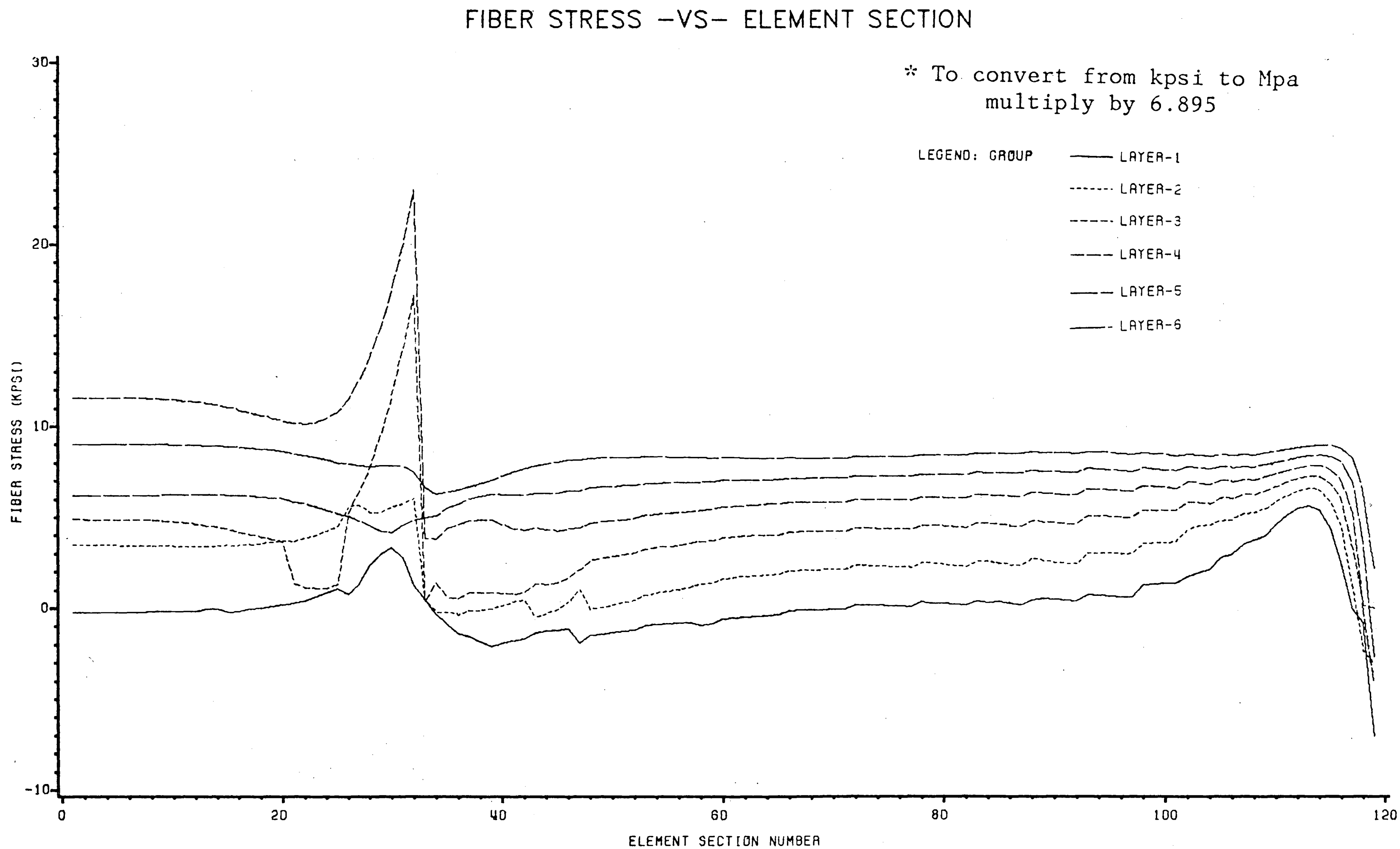

Figure 32. Layer stress curves for sand/rubber mandrel after heating.

The most obvious feature of Fig. 32 is the very high spike at section 32 (24 kpsi (165 MPa)). Comparing this curve with Fig. 29 suggests that the size of the spike and the general shape of the hoop layer curves are strong functions of the mandrel stiffness, where as the magnitude of the stress in the hoop layers is a function of the mandrel's thermal expansion coefficient.

A more important feature of Fig. 32 is that the large upward translation of all the curves as in Fig. 29 is absent. All the layers did exhibit a slight increase in tension, but not nearly of the same magnitude as in the steel mandrel model. A consequence of this is that much of the inner layer which was in compression after the winding stage is still in compression. This could lead to localized buckling. Again this pattern looks reasonable.

The sand/rubber model was then returned to the reference temperature at the end of the cooling cycle. Figure 33 shows the strange layer stress curves that result from this drop in temperature. The stress distribution in the cylindrical sections returned almost exactly to the post winding distribution. This is not at all similar to the steel mandrel model behavior. The softness of the sand/rubber mandrel is probably a good explanation for this behavior.

The most disturbing feature of Fig. 33 is the strange stress distribution in the dome region. The concave nature of the upper stress curves (layers 5 and 6) is due to the neglection of the shear coupling terms in the second material transformation. Including these terms would cause higher stresses to be reported in the dome region with the most prominent increase being around element section 70. This is precisely

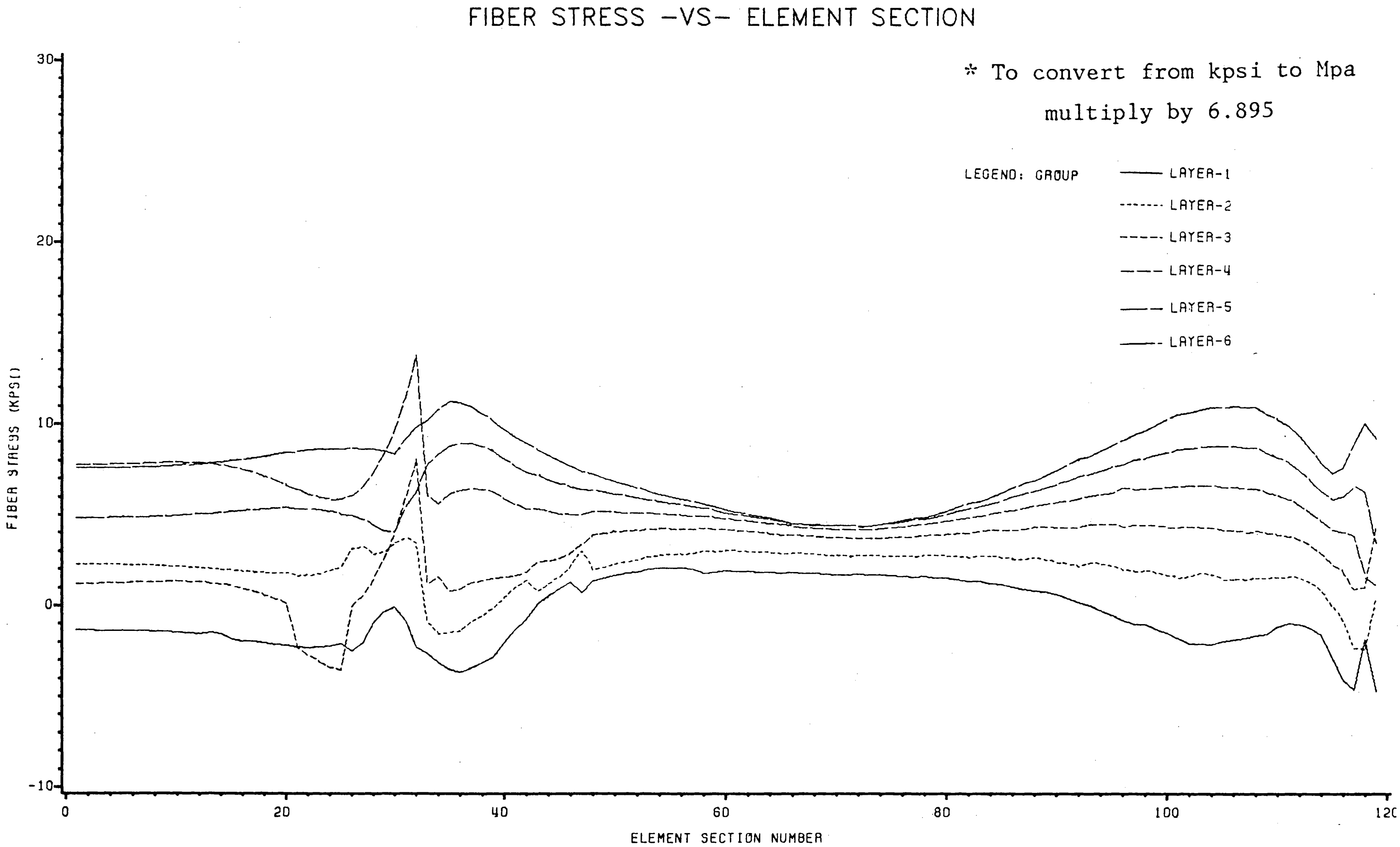

Figure 33. Layer stress curves for sand/rubber mandrel after cooling.

where the necking occurs in Fig. 33. The random behavior of the last element section is unexplainable.

Overall, the program and model seem to generate good results. More definite verification must be obtained through correlation with experimental data which is unavailable at this time.

7 CONCLUSIONS AND RECOMMENDATIONS

7.1 CONCLUSIONS

The residual stress state in a filament wound graphite/epoxy vessel after both the winding and curing stages of fabrication was determined by developing an analytical process model. The residual stress state is important because many of the defects that occur during fabrication, e.g. delamination, matrix cracking and fiber buckling, are caused by adverse residual stress states in the composite layers. Structures that contain these fabrication defects will exhibit degraded strength which make them suspect in service.

Through the development of the finite-element program WACSAFE, many of the difficulties inherent in analyzing the fabrication of composite structures were overcome. In particular, the incremental nature of the winding simulation and the orthotropic composite material properties were easily handled by the finite-element method adopted. Also, the many different materials present in the model and the need to change material properties and stress computation algorithms after cure were easily incorporated into the program.

The structure analyzed was an 18 in. (457 mm Graphite/epoxy bottle wound onto a cast sand/rubber mandrel. The finite-element model of this bottle was provided by Morton Thiokol Inc. and proved to be adequate. The addition of mandrel elements, material properties and winding data was successfully performed by the WACFORM preprocessor.

The preprocessor's graphics capabilities (geometry,material and IOFFON plots) proved invaluable in debugging and generating the complete input data file.

The relatively thin composite wall thickness (0.116 in. (2.95 mm) average) for this model did cause problems when the sand/rubber mandrel was replaced with a rigid steel mandrel. In this test case the combination of mandrel stiffness and composite thickness was insufficient to generate significant tension loss after winding. However, the less rigid sand/rubber mandrel did exhibit the predicted pattern of tension loss after winding. The termination of the hoop layers near the transition from the cylindrical wall to the dome was identified as an area where high stresses may be generated.

The two step cure simulation generated predictable results for the steel mandrel case and reasonable results for the sand/rubber mandrel. The most important conclusion drawn from the steel mandrel results is that the hoop wound fibers are subjected to a much greater stress then the surrounding helical fibers and that fiber breakage in the hoop fibers is possible if the stress generated exceeds the ultimate strength of the fiber. For the sand/rubber mandrel, the combination of thermal expansion coefficients and material stiffnesses prevented the large increase in fiber tension found in the steel model. Therefore, the inner composite layer did not recover any fiber tension at the end of the heating cycle. If the material is assumed to cure at the end of the heating cycle, then this layer would probably contain buckled fibers.

The change to cured properties and stress computations at the beginning of the cooling cycle exposed several short comings of the analytical model. First, the large compressive stresses generated in the composite layers by the contracting steel mandrel are in error because the mandrel would pull away from the polymerized composite shell. Secondly, for the sand/rubber model, the shear coupling terms will make a significant contribution to the stress state at the end of cooling. This is evidenced by the neck in the layer stress curves in Fig. 33.

The overall performance of the analytic model was better then expected for the particular model analyzed. Correlation with experimental data should provide substantiate the conclusions drawn.

7.2 RECOMMENDATIONS

Based on the results presented and the conclusions drawn, the improvements outlined in the following paragraphs are recommended.

The finite-element model could be improved by refining the mesh to better approximate the true layer boundaries. This would could be accomplished in two ways. (1) The mesh provided could be refined at Morton Thiokol Inc. or, (2) an entirely new model geometry generator could be developed.

The mandrel elements added to the model are limited to the thickness used in this work because the radial element boundary lines converge causing non-positive element stiffness to be computed. If the solid mandrel could be incorporated into the mesh at Morton Thiokol Inc. the results for the sand/mandrel model would be better.

The winding simulation could be improved by including a resin flow model other then simply using reduced winding tension and radial stiffness properties as was done in this analysis. Also, the no slip bond between the composite and the mandrel needs to be removed to better approximate the true model behavior.

More elements of the cure model need to be incorporated into the program to more closely model the continuously changing material behavior during heating and after polymerization. The assumption that all the layers cure simultaneously could easily be removed. However, this assumption was good for this analysis because there would be a uniform temperature distribution in the composite due to the thin wall. Improved material property values (especially for Poisson's ratio) should be used if located.

The shear coupling terms in the second material transformation need to be added to the program to eliminate the necking behavior of the last test case.

The most important recommendation is to obtain or generate experimental data for model verification. Since the program is capable of handling general axisymmetric shapes, the best approach would be to locate data from a commercial manufacturer such as Morton Thiokol Inc. and build or obtain a finite-element model to analyze the existing structure.

REFERENCES

1. Knight C.E., and Leavesley P.J., "An Analytical Model of Strength Loss in Filament Wound Spherical Vessels", Y/Sub/80-7733/2&01, Union Carbide Corporation, Nuclear Division, Oak Ridge Y-12 Plant, September, 1983.

2. Clough, R.W., and Woodward, R.J., III, "Analysis of Embankment Stresses and Deformations", J.Soil.Mech.Found.Div., Proc.Am.Soc.Civ.Eng., July, 1967.

3. Duncan, J.M. and Clough, G.W., "Finite Element Analysis of Port Allen Lock", J.Soil.Mech.Found.Div., Proc.Am.Soc.Civ.Eng., August, 1971.

4. Dobie, M.J., Knight, C.E., and Leavesly, P.J., "Residual Strain and Strength Loss in Filament Wound Rings", Y/Sub/80-7733/2&01, Union Carbide Corporation, Nuclear Division, Oak Ridge Y-12 Plant, August, 1982.

5. Tarnopol'skii, Y.M., Portnov, and G.G., Beil', A.I., "Technological Problems in Composite Winding Mechanics", Composite Mechanics, pp. 187-222, 1975.

6. Uemura, M., and Yamaguchi, Y., "Thermal Residual Stresses in Filament-Wound Carbon-Fiber-Reinforced Composites", J.Therm.Stresses, Vol. 2, pp. 393-412, 1979.

7. Reddy, J.N., An Introduction to the Finite Element Method, McGraw-Hill Book Company, 1984.

8. Zienkiewicz, O.C., The Finite Element Method, McGraw-Hill Book Company, 1977.

9. Allaire, P.E. Basic Finite Element Analysis, (unpublished collection of notes), 1979.

10. Cook, R.D., Concepts and Applications of Finite Element Analysis, John Wiley and Sons Inc., 1981.

11. Bathe, K.J., Finite Element Procedures in Engineering Analysis, Prentice Hall Inc., 1982.

12. Johnson, J.C., and Knight, C.E., "WACSAFE/WACFORM Program Users Guide", VPI&SU Dept.Mech.Eng.Report, January, 1986.

13. Tsai, S.W., "Mechanics of Composite Materials Part II - Theoretical Aspects", Technical Report AFML-TR-66-149 Part II, Air Force Materials Laboratory, Wright Patterson Air Force Base, Ohio, 1966.

14. TASS Finite Element Program and Preprocessor, Property of Morton Thiokol Inc., Wasatch Div.

The vita has been removed from the scanned document